Article

Targeting Mitochondria in Tumor-Associated Macrophages using a Dendrimer Conjugated TSPO Ligand Stimulates Anti-Tumor Signaling in Glioblastoma

Anjali Sharma, Kevin Liaw, Rishi Sharma, Ajit G. Thomas, Barbara S. Slusher, Sujatha Kannan, and Rangaramanujam M. Kannan

Biomacromolecules, **Just Accepted Manuscript** • DOI: 10.1021/acs.biomac.0c01033 • Publication Date (Web): 06 Aug 2020

Targeting Mitochondria in Tumor-Associated Macrophages using a Dendrimer Conjugated TSPO Ligand Stimulates Anti-Tumor Signaling in Glioblastoma

*Anjali Sharma,[1§] Kevin Liaw,[1,2§] Rishi Sharma,[1] Ajit G. Thomas,[3] Barbara S. Slusher,[3-9] Sujatha Kannan,[1,10,11] and Rangaramanujam M. Kannan[*1,2,11]*

[1]Center for Nanomedicine, Department of Ophthalmology, Wilmer Eye Institute

[2]Department of Chemical and Biomolecular Engineering

[3]Johns Hopkins Drug Discovery

[4]Department of Neurology

[5]Department of Neuroscience

[6]Department of Medicine

[7]Department of Oncology

[8]Department of Psychiatry and Behavioral Sciences

[9]Department of Pharmacology and Molecular Sciences

[10]Department of Anesthesiology and Critical Care Medicine,

[11]Hugo W. Moser Research Institute at Kennedy Krieger

[§]These authors contributed equally

*Corresponding author:

Rangaramanujam M. Kannan, Arnall Patz Distinguished Professor of Ophthalmology, Center for Nanomedicine at the Wilmer Eye Institute, 400 North Broadway, Baltimore, Maryland 21231, USA; Email: krangar1@jhmi.edu; Phone: 443-287-8634.

Abstract

Mitochondria mediate critical cellular processes, including proliferation, apoptosis, and immune responses; as such, their dysfunction is pathogenic in many neurodegenerative disorders and cancers. In glioblastoma, targeted delivery of mitochondria-focused anti-cancer therapies have failed to translate into clinical successes due to their nonspecific cellular localization, heterogeneity of receptor expression across patients, poor transport across biological barriers to reach the brain, tumor, and mitochondria, as well as systemic side effects. Strategies that can overcome brain and solid tumor barriers and selectively target mitochondria within specific cell types may yield improvements to glioblastoma treatment. Developments in dendrimer-mediated nanomedicines have shown promise targeting tumor-associated macrophages (TAMs) in glioblastoma following systemic administration. Here, we present a novel dendrimer conjugated to the translocator protein 18KDa (TSPO) ligand 5,7-dimethylpyrazolo[1,5-α]pyrimidin-3-ylacetamide (DPA). We developed a clickable DPA for conjugation on dendrimer surface and demonstrate *in vitro* that the dendrimer-DPA conjugate (D-DPA) significantly increases dendrimer co-localization with mitochondria. Compared to free TSPO ligand PK11195, D-DPA stimulates greater anti-tumor immune signaling. *In vivo*, we show that D-DPA targets mitochondria specifically within TAMs following systemic administration. Our results demonstrate that dendrimers can achieve TAMs specific targeting in glioblastoma and can be

further modified to target specific intracellular compartments for organelle-specific drug delivery.

Keywords

Dendrimer, Glioblastoma, Tumor-associated macrophages, mitochondria, targeting

Introduction

The mitochondrion is widely known as the powerhouse of the cell and is chiefly responsible for regulating cellular energy production and metabolism.[1] In addition, mitochondria play critical roles in regulating trafficking, proliferation, apoptosis, and immune responses.[2] Due to their position at the nexus of these vital physiological functions, mitochondrial dysfunction is associated with diverse diseases ranging from neurodegenerative disorders to cancers to autoimmune disorders.[3, 4] Restoration of healthy mitochondrial function from pathological activity is therefore necessary to address progression of these diseases.[5]

Defective mitochondria function in cell cycle regulation and apoptotic signaling is characteristic of cancer progression.[6] Therefore, intracellular targeting anti-cancer therapies focused on mitochondria to slow cancer cell proliferation and induce apoptosis have been explored.[7] In addition, due to their roles in mediating inflammatory responses, mitochondria have also been explored as targets in cancer immunotherapy approaches.[8] For example, mitochondrial damage in T cells have been found to mediate suppression of anti-cancer immune response.[9, 10] Tumor-associated macrophages (TAMs) have been found to mediate the cancer immune response, and their activation state has been shown to be regulated by mitochondrial metabolism.[11, 12] Mitochondria mediate HIF-1α and HIF-2α in TAMs, and their localization to mitochondria correlates with high grade and poor prognoses of cancers.[11] In addition,

dysfunctional mitochondria exhibit overproduction of reactive oxygen species, leading to high oxidative stress in the tumor environment that promotes tumor growth.[13, 14] As a therapeutic target in TAMs, mitochondria can be leveraged to promote anti-tumor signaling by activating pro-inflammatory immune signaling.[15] However, TAMs-focused immunotherapies have suffered from low response rates, poor brain and tumor penetration, and non-selective activity resulting in systemic toxicities that have hampered their clinical translation.[16, 17] In addition, the failure of mitochondria-targeted therapies lies largely with their inability to preferentially accumulate in mitochondria of specific cells of interest. Therefore, a nanotechnology-mediated strategy aimed at cell-specific mitochondrial targeting may overcome these delivery challenges as an effective treatment for glioblastoma and other cancers.[8]

Translocator protein 18 kDa (TSPO) is a transport protein located on the outer mitochondrial membrane that is responsible for transporting cholesterol into mitochondria for synthesis of steroids.[18] TSPO is minimally expressed in healthy tissues, but is highly overexpressed in the context of neuroinflammation and cancer.[19, 20] In the context of glioblastoma, TSPO expression correlates with glioblastoma clinical outcomes.[21] Targeting TSPO has been explored to improve diagnostics through positron-emission tomography (PET) imaging and therapies.[22, 23] TSPO is highly upregulated in anti-inflammatory macrophages consistent with the immunosuppressive TAMs phenotype.[24] Targeting TSPO can leverage its overexpression in TAMs to manipulate immune polarization. PK11195 is a first generation TSPO ligand with nanomolar binding affinity that has been extensively explored as an inhibitor of tumor cell proliferation and modulator of immune signaling.[25, 26] 5,7-Dimethylpyrazolo[1,5-α]pyrimidin-3-ylacetamide (DPA) is a novel class of TSPO ligands which are selective, drug-like ligands.[27] While these TSPO targeting compounds have been explored extensively for

diagnostics in PET imaging, their utility for targeted drug delivery in the brain have been limited by poor brain penetration.[28, 29] Therefore, nanomedicines that can penetrate into the brain and brain tumors may enable effective TSPO targeting for improved drug delivery.

Many nanotechnology-based strategies are being developed to target drugs to mitochondria.[30, 31] However, platforms that enable mitochondria targeting within specific cell types in the brain are still being developed. Dendrimers have shown significant promise for specific gene and drug delivery to activated microglia, cancer cells and TAMs.[31-37] In an orthotopic brain cancer models, we have previously shown that systemic administration of generation 4 hydroxyl-terminated polyamidoamine (PAMAM) dendrimers are able to fully penetrate and distribute uniformly throughout the solid brain tumor selectively in TAMs, with minimal accumulation in healthy brain and peripheral tissues.[33, 38] This cell-type specific targeting is achieved without the need for targeting ligands. This dendrimer platform has potential for clinical applications, with favorable safety profile and scalability of production.[39, 40] Here we present a novel dendrimer-DPA conjugate for specific targeting of mitochondria within TAMs as a unique immunotherapy approach. We describe the design, synthesis, chemical characterization, *in vitro* mitochondrial localization and immune repolarization, and *in vivo* targeting properties of this dendrimer-DPA conjugate.

Materials and Methods

Synthesis

Materials and reagents: 2,4-Pentanedione, borontribromide, ethyleneglycol ditosylate (**4**), sodium azide, potassium carbonate, 1-[3-(Dimethylamino)propyl]-3-ethylcarbodiimide methiodide (EDC), 4(dimethylamino)pyridine (DMAP), GABA_BOC_OH, *N*, *N*-diisopropyl

ethyl amine (DIPEA), copper sulfate pentahydrate, sodium ascorbate, and 5-Hexynoic acid, were purchased from Sigma Aldrich US. Cy5 NHS ester was purchased from GE healthcare and used as received. All the anhydrous solvents were purchased from Sigma and were used as received. Hydroxyl PAMAM dendrimer with ethylenediamine-core (generation 4, 64 hydroxyl terminal-groups, Pharma grade, compound (**7**) was purchased from Dendritech as 13 wt% methanolic solution. Methanol was evaporated using rotary evaporator prior to use. D-Cy5 was synthesized using previously published protocols.[41]

Characterization: Proton nuclear magnetic resonance spectra (NMR) were recorded using Bruker spectrometer (500 MHz). The data is reported as chemical shift (δ ppm). The peaks are relative to the residual protonated solvent resonance and are reported in terms of multiplicity (s = singlet, d = doublet, t = triplet, q = quartet, m = multiplet), coupling constants (J Hz) and assignment. High resolution mass spectra (HRMS) was recorded using electrospray ionization (ESI) recorded on a Bruker microTOF-II mass spectrometer in the positive mode. The samples were introduced via direct flow using CH_3CN/ H_2O (9:1) solvent system. The empirical formula confirmation is reported as protonated molecular ions $[M + nH]^{n+}$ or adducts [M + nX]n+ (X = Na). High pressure liquid chromatography (HPLC) was performed on a Waters system with 2998 photodiode array detector and a 2475 multi λ fluorescence detector, In-Line degasser, a 1525 binary pump and Waters Empower 2 Software. Separation was achieved on a Waters column (C18 symmetry 300, 5µm, 4.6x250mm). Flow rate was maintained at 1.0 mL/min over a gradient from 100:0 (A:B) gradually increasing to 50:50 (A:B) at 25 min, 10:90 (A:B) at 35 minutes, and finally returning to 100:0 (A:B) at 40 minutes maintaining a flow rate of 1 mL/min. (A: 0.1% TFA and 5% ACN in water and buffer B: 0.1% TFA in ACN) and eluent monitored at wavelengths 210 and 650 nm. Flash chromatography was performed using Teledyne combiflash

sytem. Size and zeta potential measurements were carried out via Dynamic light scattering using Malvern Zetasizer Nano ZS as previously reported by our group.[42]

Procedures for the synthesis of intermediates and dendrimer conjuagtes:

Synthesis of compound 2: A solution of compound **1** (500 mg, 1.65 mmoles) and 2,4-pentanedione (0.17 mL, 1.65 mmoles) in anhydrous ethanol (15mL) was heated at 60^{o}C in a microwave reactor for 20 hours. Upon completion, the solvent was evaporated and the residue was dissolved in dichloromethane (DCM). The organic layer was washed with water and brine and dried over sodium sulfate. The dried organic layer was then evaporated and the crude product was purified using combiflash. The pure fractions were obtained in 3% methanol in dichloromethane and were evaporated to afford an off-white solid product. Yield: 85%.

^{1}H NMR (500 MHz, $CDCl_3$) δ 7.86 – 7.66 (m, 2H), 7.08 – 6.87 (m, 2H), 6.51 (d, *J* = 0.7 Hz, 1H), 3.92 (s, 2H), 3.86 (s, 3H), 3.51 (q, *J* = 7.1 Hz, 2H), 3.42 (q, *J* = 7.1 Hz, 2H), 2.75 (s, 3H), 2.55 (s, 3H), 1.21 (t, *J* = 7.1 Hz, 3H), 1.12 (t, *J* = 7.1 Hz, 3H). **Figure S1**

^{13}C NMR (126 MHz, $CDCl_3$) δ 170.14, 159.81, 157.44, 155.05, 147.69, 144.70, 130.00, 126.39, 113.98, 108.15, 100.81, 77.31, 77.05, 76.80, 55.34, 42.33, 40.62, 28.21, 24.68, 16.94, 14.36, 13.11. **Figure S2**

ESI-MS: Theoretical for $C_{21}H_{26}N_4O_2$ is 366.21, observed is 367.21 $[M+1]^+$ **Figure S3**

Synthesis of compound 3: To a stirring solution of compound **2** (450 mg, 1.23 mmoles) in anhydrous DCM (5mL), 1M borontribromide in THF (6.13 mL, 5 equivalents) was added dropwise at -60^{o}C. The stirring was continued for 2 hours. Upon completion, the reaction mixture was quenched by pouring onto ice. The reaction mixture was diluted with water and the

product was extracted out in DCM. DCM layer was evaporated to afford compound **3** as yellow solid in quantitative yield.

^{1}H NMR (500 MHz, MeOD) δ 7.53 (d, *J* = 8.3 Hz, 2H), 6.95 – 6.75 (m, 3H), 3.98 (s, 2H), 3.54 (q, *J* = 7.1 Hz, 2H), 3.42 (q, *J* = 7.1 Hz, 2H), 2.83 (d, *J* = 7.6 Hz, 3H), 2.64 (s, 3H), 1.32 – 1.18 (m, 3H), 1.13 (t, *J* = 7.1 Hz, 3H). **Figure S4**

^{13}C NMR (126 MHz, MeOD) δ 172.5, 160.27, 156.99, 129.79, 115.12, 100.35 – 98.18, 42.24, 40.70, 27.43, 21.56, 15.86, 12.88, 11.85. **Figure S5**

ESI-MS: Theoretical for $C_{20}H_{24}N_4O_2$ is 352.19, observed is 353.19 $[M+1]^+$ **Figure S6**

Synthesis of compound 5: To a stirring solution of compound **4** (3 g, 8.1 mmoles) in DMF, sodium azide (790 mg, 12.15 mmoles) was added and the reaction mixture was heated at 40^{o}C for 24 hours. Upon cooling to ambient temperature, the reaction mixture was diluted with ethylacetate and washed with water. The organic layer was dried over sodium sulfate and evaporated. The crude product was purified via combiflash using 30% ethylacetate in hexanes. The product was obtained as a transparent liquid. Yield: 60%.

^{1}H NMR (500 MHz, $CDCl_3$) δ 7.82 (d, *J* = 8.3 Hz, 2H), 7.37 (d, *J* = 8.1 Hz, 2H), 4.24 – 4.06 (m, 2H), 3.49 (t, *J* = 5.1 Hz, 2H), 2.46 (s, 3H). **Figure S7**

^{13}C NMR (126 MHz, $CDCl_3$) δ 145.26, 132.63, 130.00, 128.00, 68.04, 49.62, 21.71, 0.02.

Figure S8

Synthesis of compound 6 (DPA-azide): To a stirring solution of compound 3 (360 mg, 1.02 mmoles) in anhydrous anhydrous tetrahydrofuran (THF, 5mL), potassium carbonate (705 mg, 5.11 mmoles) was added and the stirring was continued for 30 minutes followed by the addition

of compound **5** (344.5 mg, 1.42 mmoles) in DMF (2mL). The reaction mixture was stirred at 50^{o}C for overnight. Upon completion, the solvent was evaporated. The residue was dissolved in ethylacetate and washed with water. Column purification was performed to afford the pure product. Yield: 82%

^{1}H NMR (500 MHz, $CDCl_3$) δ 7.85 – 7.74 (m, 2H), 7.08 – 6.93 (m, 2H), 6.51 (d, *J* = 0.5 Hz, 1H), 4.26 – 4.15 (m, 2H), 3.93 (s, 2H), 3.62 (t, *J* = 5.0 Hz, 2H), 3.51 (q, *J* = 7.1 Hz, 2H), 3.41 (q, *J* = 7.1 Hz, 2H), 2.75 (s, 3H), 2.55 (s, 3H), 1.21 (t, *J* = 7.1 Hz, 3H), 1.11 (t, *J* = 7.1 Hz, 3H). **Figure S9**

^{13}C NMR (126 MHz, $CDCl_3$) δ 170.03, 158.46, 157.49, 130.11, 127.07, 114.68, 108.18, 100.91, 77.29, 77.04, 76.78, 67.00, 50.21, 42.34, 40.63, 28.19, 24.55, 16.97, 14.38, 13.12, 0.02. **Figure S10**

ESI-MS: Theoretical for $C_{22}H_{27}N_7O_2$ is 421.22, observed is 422.23 $[M+1]^+$ **Figure S11**

Synthesis of compound 8: To a stirring solution of compound **7** (800mg, 0.056 mmoles) in anhydrous DMF (10mL), pentynoic acid (82.44 mg, 0.840 mmoles) was added followed by the addition of DMAP (108.12mg, 0.885 mmoles) and EDC (169.65mg, 0.885mmoles). The reaction mixture was stirred at room temperature for 24 hours. This was followed by the dialysis against DMF and then water. The aqueous solution was lyophilized to yield compound **8** as a hygroscopic white solid. Yield: 82%

^{1}H NMR (500 MHz, DMSO) δ 8.10-7.62 (D-N*H*-CO), 4.71 (s, D-OH), 4.03 (t, D-CH_2-COO), 3.49-3.22 (m, D-CH_2), 3.18-2.94(m, D-CH_2), 2.78 (s, linker -C≡CH), 2.82-2.55 (m, D-CH_2), 2.45-2.30 (m, D-CH_2), 2.29-2.18 (m, D-CH_2). **Figure S12**

Synthesis of compound 9: To a stirring solution of compound **8** (500 mg, 0.033 mmoles) in anhydrous DMF (10mL), BOC-GABA-OH (33 mg, 0.166 mmoles) was added followed by the addition of DMAP (24.1 mg, 0.198 mmoles) and EDC (37.8 mg, 0.198 mmoles). The reaction mixture was stirred at room temperature for 24 hours. This was followed by the dialysis against DMF and then water. The aqueous solution was lyophilized to yield compound **9** as a hygroscopic white solid. Yield: 82%

^{1}H NMR (500 MHz, DMSO) δ 8.19-7.68 (D-N*H*-CO), 4.72 (s, D-OH), 4.09-4.34 (m, D-C*H*$_2$-COO), 3.53-3.00 (m, D-C*H*$_2$), 2.80-2.57 (m, D-C*H*$_2$), 2.47-1.92 (m, D-C*H*$_2$), 1.62 (t, linker –CH_2), and 1.37 (BOC H). **Figure S13**

Synthesis of compound 10: A solution of compound 9 (400mg) in 30% trifluoroacetic acid (TFA) in DCM was stirred vigorously for 12 hours. The solution was co-evaporated with methanol to remove TFA to afford compound **10** as hygroscopic solid in quantitative yield which was used directly for next step.

^{1}H NMR (500 MHz, DMSO) δ 8.19-7.64 (D-N*H*-CO), 4.71 (s, D-OH), 4.09 (m, D-C*H*$_2$-COO), 4.02 (m, D-C*H*$_2$-COO), 3.53-3.00 (m, D-C*H*$_2$), 2.78 (s, linker -C≡CH), 2.85-2.53 (m, D-C*H*$_2$), 2.46-2.07 (m, D-C*H*$_2$), 1.72 (t, linker –CH_2). **Figure S14**

Synthesis of compound 11*:* To a stirring solution of compound **10** (403 mg, 0.026 mmoles) and compound **6** (165.45 mg, 0.392 mmoles) in DMF/THF mixture, a solution of $CuSO_4.5H_2O$ (1mg, 0.004mmoles) in water (1mL) was added. This was followed by the addition of sodium ascorbate (1.5mg, 0.008 mmoles) in water (1mL). The reaction mixture was left to stir overnight at 40^{o}C. The aqueous solution was lyophilized to afford compound **11** as white solid. Yield: 83%.

^{1}H NMR (500 MHz, DMSO) δ 8.05-7.67 (D-N*H*-CO), 7.65-7.56 (m, DPA ArH), 7.00-6.90 (m, DPA ArH), 6.77-6.71 (m, DPA ArH), 4.66 (DPA H), 4.35 (DPA H), 4.06-3.94 (m, D-CH_2-COO), 3.79-3.72 (m, linker-CH_2), 3.50-3.11 (m, D-CH_2), 3.11-2.89 (m, D-CH_2), 2.38-2.25 (m, D-CH_2), 2.22-1.99 (m, D-CH_2), 1.10 (t, DPA –CH_3), 0.93 (t, DPA –CH_3). **Figure S15**

Synthesis of compound 12 (DPA-D-Cy5): To a stirring solution of compound **11** (193 mg, 0.009 mmoles) in DMF, Cy5-NHS ester (12.13 mg, 0.019 mmoles) was added at pH 7.5. The reaction mixture was left to stir overnight at room temperature. The solution was then dialyzed against DMF followed by water. The aqueous solution was lyophilized to afford compound **12** as a blue solid. Yield: 72%.

^{1}H NMR (500 MHz, DMSO) δ 8.39-8.29 (m, Cy5H), 8.13-7.74 (D-N*H*-CO), 7.72-7.63 (m, DPA ArH), 7.34-7.27 (m, Cy5H), 7.04-6.96 (m, DPA ArH), 6.82-6.75 (m, DPA ArH), 6.62-6.52 (m, Cy5H), 6.32-6.21(m, Cy5H), 4.9-4.56 (m, DPA H), 4.48-4.28 (m, DPA H), 4.05-3.94 (m, D-CH_2-COO), 3.87-3.75 (m, linker-CH_2), 3.50-3.19 (m, D-CH_2), 3.18-3.00 (m, D-CH_2), 2.72-2.57 (m, D-CH_2), 2.31-2.011 (m, D-CH_2).76-1.62 (Cy5H), 1.44-0.89 (DPA –CH_3, linker H and Cy5H). **Figure S16**

HPLC: Retention time: 23.1 minutes, Purity: 99.8% **Figure S17**

Synthesis of compound 13 (D-DPA): To a stirring solution of compound **8** (500 mg, 0.033 mmoles) and compound **6** (165.45 mg, 0.392 mmoles) in DMF/THF mixture, a solution of $CuSO_4.5H_2O$ (1mg, 0.004mmoles) in water (1mL) was added. This was followed by the addition of sodium ascorbate (1.5mg, 0.008 mmoles) in water (1mL). The reaction mixture was left to stir overnight at 40^{o}C. The aqueous solution was lyophilized to afford compound **13** as white solid. Yield: 87%.

^{1}H NMR (500 MHz, DMSO) δ 8.09-7.73 (D-N*H*-CO), 7.72-7.62 (m, DPA ArH), 7.04-6.98 (m, DPA ArH), 6.85-6.77 (m, DPA ArH), 4.73 (t, DPA H), 4.43 (DPA H), 4.00 (m, D-C*H*$_2$-COO), 4.82 (t, DPA H), 3.50 (m, DPA H), 3.48-2.97 (m, linker-C*H*$_2$), 2.73-2.57 (m, D-C*H*$_2$), 2.28-2.07 (m, D-C*H*$_2$), 1.84 (t, linker H), 1.17 (t, DPA –CH$_3$), 1.01 (t, DPA –CH$_3$). **Figure S18**

HPLC: Retention time: 24.2 minutes, Purity: 99% **Figure S19**

Synthesis of D-DPA: The synthetic protocol for the synthesis of DPA-triazole is described in supplementary section. The ^{1}H and ^{13}C NMR spectra for DPA-triazole are presented in **figures S20 and S21**.

Biology studies

Materials

DMEM media, RPMI media, fetal bovine serum (FBS), penicillin-streptomycin (P/S), 0.25% trypsin-EDTA, NucBlue fixed cell stained, goat anti-rabbit Alexafluor 488, TRIzol, and MTT reagent were purchased from Invitrogen (Carlsbad, CA, USA). Lysine-coated glass bottom dishes were purchased from MatTek Inc. (Ashland, MA, USA). Anti-AIF antibody was purchased from Abcam (Cambridge, UK). Methanol, 4% formalin solution, Triton-X, bovine serum albumin (BSA), and lipopolysaccharide (LPS) were purchased from Sigma Aldrich (St. Louis, MO, USA). Mitochondria isolation for mammalian cells kit and normal goat serum (NGS) were purchased from ThermoFisher (Waltham, MA, USA). Lectin Dylight 594 was purchased from Vector Laboratories Inc. (Burlingame, CA, USA). Phosphate buffered saline (PBS) and tris buffered saline (TBS) were obtained from Corning Inc. (Corning, NY, USA).

Mitochondrial isolation

To assess comparative binding affinities, mitochondria were isolated from kidneys and adrenal glands harvested from neonatal rabbits. These tissues were chosen because TSPO has been shown to have high expression in steroid producing tissues such as adrenal glands.[68] Mitochondrial isolation was performed using a mitochondria extraction from mammalian tissues kit as per manufacturer's procedure (ThermoFisher).

TSPO binding affinity of D-DPA

Binding of compounds to the TSPO receptor were evaluated using a radiolabeled membrane binding assay in tandem with size exclusion chromatography. [^{3}H]-PK11195 (Cat# NET885250UC, Perkin Elmer, Boston, MA) was used as the radioligand and mitochondria, as isolated above, used as the receptor source. Briefly, mitochondria were incubated with a range of concentrations of the tested compounds (1 pM – 100 µM) and [^{3}H]-PK11195 (1.2 nM) in 50 mM Tris.HCl buffer at pH 7.4 and in a total volume of 100 µl for 30 min and at room temperature (RT). Total binding was determined in the presence of [^{3}H]-PK11195 alone and non-specific binding was determined in the presence of both [^{3}H]-PK11195 and 100 nM unlabeled PK11195. At the end of the incubation period, 90 µl of the reaction mixture was transferred to pre-equilibrated, 7K molecular weight cut off, 96-well, Zeba Spin Desalting plates (Cat# 89807, Thermo Scientific, Rockford, IL). [^{3}H]-PK11195-bound mitochondria was eluted upon centrifugation at 1000 x g for 2 min (Beckman GS-6R centrifuge with PTS-200 swinging bucket rotor) and the radioactivity in 80 µl of the flow through detected using solid scintillator-coated 96-well LumaPlates (Perkin Elmer, Cat# 6005630) in conjunction with Perkin Elmer's TopCount instrument. Finally, IC_{50} values were determined from CPM results of the specific binding using Microsoft Office Excel, IDBS' XLfit and GraphPad Prism programs.

Cell culture

HMC3 human macrophages were acquired from ATCC (Manassas, VA, USA). BV2 murine microglia were obtained from the Children's Hospital of Michigan's cell culture facility. GL261 murine glioblastoma cells were obtained from the DTP/DCTD/NCI Tumor Repository (Frederick, MA, USA). HMC3 and BV2 cells were maintained in DMEM supplemented with 10% FBS and 1% P/S. GL261 cells were maintained in low glutamine RPMI supplemented with 10% FBS, 1% P/S, and 1% L-glutamine. Cells were kept at 37ºC in 5% CO_2 atmosphere. Treatments were performed in half serum media (5% FBS).

Mitochondrial colocalization and quantification

Imaging and colocalization of mitochondria with dendrimers were performed according to previously published protocols.[41] Briefly, HMC3 macrophages were seeded on glass bottom culture dishes. HMC3 cells were used to image mitochondrial targeting due to their large cell bodies. Cells were treated with fluorescently labeled dendrimer (D-Cy5) and DPA-conjugated dendrimer (Cy5-D-DPA) for 48 hours at 50 µg/mL. Cells were then fixed in 4% formalin solution. Cells were stained with rabbit anti-mouse AIF primary antibody (1:200) and anti-rabbit Alexafluor 488 (1:200) to label mitochondria, Lectin Dylight 594 to label cell membranes, and DAPI to label cell nuclei.

For quantification of dendrimer content in isolated mitochondria, BV2 murine microglia were used due to greater yield of isolated mitochondria. Dendrimer quantification from cell extracts were performed as described previously with modifications for mitochondrial isolation.[69] Cells were treated with 50 µg/mL D-Cy5 or Cy5-D-DPA for 24 hours. Cells were freshly fractionated to yield isolated mitochondria and cytosolic fractions. Isolated mitochondria were then resuspended in isolation buffer, and dendrimers were extracted via three freeze/thaw cycles with liquid nitrogen. Dendrimer fluorescence in each fraction was measured using a

Shimadzu RF-3501PC spectrofluorophotometer (Shimadzu Corporation, Columbia, MD, USA). Fluorescence intensities were converted into masses using calibration curves of known dendrimer concentrations.

Analysis of inflammatory expression

BV2 murine microglia were stimulated with LPS at 300 EU/mL for 3 hours, followed by cotreatment with PK11195 or DPA-conjugated dendrimer (D-DPA) with LPS for 24 hours. Then, cells were exposed to fresh media for 24 hours and collected for analysis of cellular and extracellular signals. LPS was chosen as a stimulant despite induction of pro-inflammatory immune response due to its role in mediating cancer cell metastasis, proliferation, and immune recruitment.[41, 42, 70] Cells were collected in TRIzol and mRNA extracted according to manufacturer's procedure. cDNA conversion was then performed using a cDNA conversion kit (ThermoFisher) and thermocycler (Bio-Rad Laboratories, Hercules, CA, USA). Cells were then analyzed for immune expression using rt-qPCR StepOne Plus system (Applied Biosystems). Primer sequences used were as follows: TNFα (F: CCA GTG TGG GAA GCT GTC TT; R: GTG TAA TTA AGC CTC CGA CTT G), IL1β (F: AGC TTC AAA TCT CGA AGC AG; R: TGT CCT CAT CCT GGA AGG TC), arginase-1 (F: TCA TGG AAG TGA ACC CAA CTC TTG; R: TCA GTC CCT GGC TTA TGG TTA CC), and GAPDH (F: TGT CGT GGA GTC TAC TGG TGT CTT C; R: CGT GGT TCA CAC CCA TCA CAA). Cell supernatants were assessed for TNFα and nitrite secretion using mouse TNFα Quantikine ELISA kit (R&D Systems, Minneapolis, MN, USA) and Griess reagent assay kit (Promega, Madison, WI, USA) according to manufacturer's procedure, respectively. Samples were read on a Synergy Mx microplate reader (BioTek, Winooski, VT, USA). Cytotoxicity of D-DPA compared to PK11195 was assessed using MTT assay.

Tumor inoculations

All animals were housed at the Johns Hopkins University animal facilities and were given free access to food and water. All animal experiments were conducted in accordance with protocols approved by the Johns Hopkins University institutional animal care and use committee.

To establish the GL261 orthotopic immunocompetent model of glioblastoma, male and female C57BL/6 (Jackson Laboratory, Bar Harbor, ME, USA) mice 6-8 weeks of age were intracranially implanted with GL261 cells. Cells were brought to a concentration of 100,000 cells per 2 µL. Mice were anesthetized using a ketamine/xylazine for survival surgeries. A midline scalp incision was created, and a burr hole was drilled 1 mm posterior to the bregma and 2 mm lateral to the midline to inject cells into the striatum. A 2 µL Hamilton syringe (Hamilton Company, Reno, NV, USA) was lowered to a depth of 2.5 and injected 2 µL of cell solution over 10 minutes with an automated syringe pump (Stoelting Co., Wood Dale, IL, USA). The syringe was withdrawn slowly. The incision was sutured together, and antibiotic cream was applied to the wound.

To determine TSPO overexpression in this model of glioblastoma, tumors and contralateral hemisphere tissues were dissected from brains collected 14 days after tumor inoculation. Tissues were processed for mRNA extraction and rt-qPCR as described above, with additional agitation initially to dissociate tissues. Premade TSPO primers were obtained from Bio-Rad.

To assess systemic biodistribution of Cy5-D-DPA compared to D-Cy5, glioblastoma brain tumor bearing mice were intravenously injected with dendrimers at 55 mg/kg on day 14 post inoculation. Clearance organs (kidney, liver, spleen) were collected 24 hours later after

perfusion. Organs were dissected into equivalent mass samples and homogenized with stainless steel beads in a bullet blender homogenizer (Next Advance Inc., Troy, NY, USA) to extract dendrimers into methanolic solution. Fluorescence was measured using the spectrofluorophotometer and converted to quantities using calibration curves of known dendrimer concentration.

Tissue processing and immunohistochemistry

Glioblastoma brain tumor bearing mice were injected intravenously with D-Cy5 or Cy5-D-DPA on day 14 post-inoculation. Mice were perfused and brain collected 24 hours after injection. Brains were fixed in 4% formalin solution, followed by sucrose gradient to remove residual formalin (10%, 20%, then 30% sucrose in PBS overnight each). Brains were sectioned axially into 30 µm using a Leica CM 1905 cryostat (Wetzlar, Germany). Brains were stained with DAPI to label nuclei, Iba1 (1:200) to label TAMs, and AIF (1:200) to label mitochondria. Slices were blocked in 1x TBS + 0.1% Triton-X + 1% BSA + 5% NGS for 4 hours at room temperature. Slices were then incubated with primary antibodies diluted in 1x TBS + 0.1% Triton-X + 1% BSA overnight at 4ºC. Then slices were washed and incubated with secondary antibodies (goat anti-rabbit 488) for 2 hours at room temperature. Finally, slices were incubated with DAPI for 15 minutes, mounted, and sealed.

Confocal imaging

Images were acquired using a Zeiss LSM710 confocal microscope (Hertfordshire, UK). Background fluorescence in cells and tissues were set with untreated samples. Microscope settings such as laser intensity, gain, and offset were kept constant across compared images. Zenlite 2011 software was used to process the obtained images, and any adjustments to

brightness and contrast were kept constant across all compared images. Colocalization and fluorescence profiles were obtained with the Zenlight 2011 software.

Statistical analyses

Graphs and statistical analyses were performed using GraphPad Prism v8.0 software (San Diego, CA, USA). Error bars presented represent mean ± standard errors. Statistical significance between colocalization coefficients was determined with Student's t-test. Significances in comparisons between PK11195 and D-DPA were performed with two-way ANOVAs.

Results

Synthesis of the dendrimer-DPA conjugate and intermediates

To enable mitochondria targeting within TAMs in glioblastoma, DPA was conjugated to generation 4 hydroxyl-terminated polyamidoamine dendrimers via non-cleavable linkages. Chemical conjugation of DPA on the surface of dendrimer is challenging due to the absence of functional groups that can be easily modified to attach a linker. To address this issue, we first synthesized a conjugable form of DPA (**Figure 1A**) with azide terminal group separated by a two carbon linker. This served two purposes, i) the presence of an azide terminal group participated in copper (I) catalyzed alkyne-azide click (CuAAC) reaction on dendrimer surface, and ii) the resulting aromatic triazole ring with the two carbon spacer for enhanced TSPO binding affinity, as modifications with phenethyl ether side-chains have resulted in DPA analogs with highest TSPO binding affinities.[27] The synthesis of DPA-azide began with the condensation of compound **1** with 2,4 pentanedione to generate pyrazolopyrimidine derivative **2**, which on subsequent cleavage of methoxy group with borontribromide afforded phenolic derivative **3**. The two carbon orthogonal linker was synthesized by mono-azidation of ethyleneglycol ditosylate **4**

to afford linker **5**. The phenolic intermediate **3** was subsequently reacted with **5** using potassium carbonate and mild heating to afford clickable version of DPA as DPA-azide (**6**). To enable fluorescent imaging of DPA-conjugated dendrimers, the dendrimer surface was functionalized with two orthogonal functional groups to obtain a trifunctional dendrimer for the simultaneous conjugation of a cyanine 5 (Cy5) fluorescent probe and DPA (**Figure 1B**). Using simple esterification reactions, dendrimers (**7**) were first modified with pentynoic acid to bring alkyne groups to enable click reaction with azide-terminated DPA (**6**). The alkyne-terminating dendrimer **8** was then modified in two steps by first reacting with GABA-BOC-OH followed by BOC deprotection in mild acidic conditions, to afford amine groups to enable conjugation to Cy5-NHS ester, resulting in trifunctional dendrimer with two orthogonal functional groups for further attachment (**10**). The alkyne groups in trifunctional dendrimer **10** were further reacted with DPA-azide (**6**) via CuAAC click reaction to afford dendrimer **11**, which was subsequently reacted with Cy5-NHS via activated acid-amine coupling reaction to obtain the final fluorescently labeled dendrimer-DPA conjugate (**12**). For binding and efficacy studies, a non-fluorescently labeled dendrimer-DPA conjugate was synthesized by simply reacting alkyne-terminating dendrimer **8** with DPA-azide (**6**) to afford D-DPA (**13, Figure 1C**). We conjugated only ~9 molecules of DPA (19%w/w) on the surface of hydroxyl dendrimer to keep the inherent biodistribution and targeting potential of the parent dendrimer intact. In addition, for comparison purpose, we also synthesized a DPA-triazole analogue by reacting DPA-azide with propargyl alcohol (**Scheme S1**).

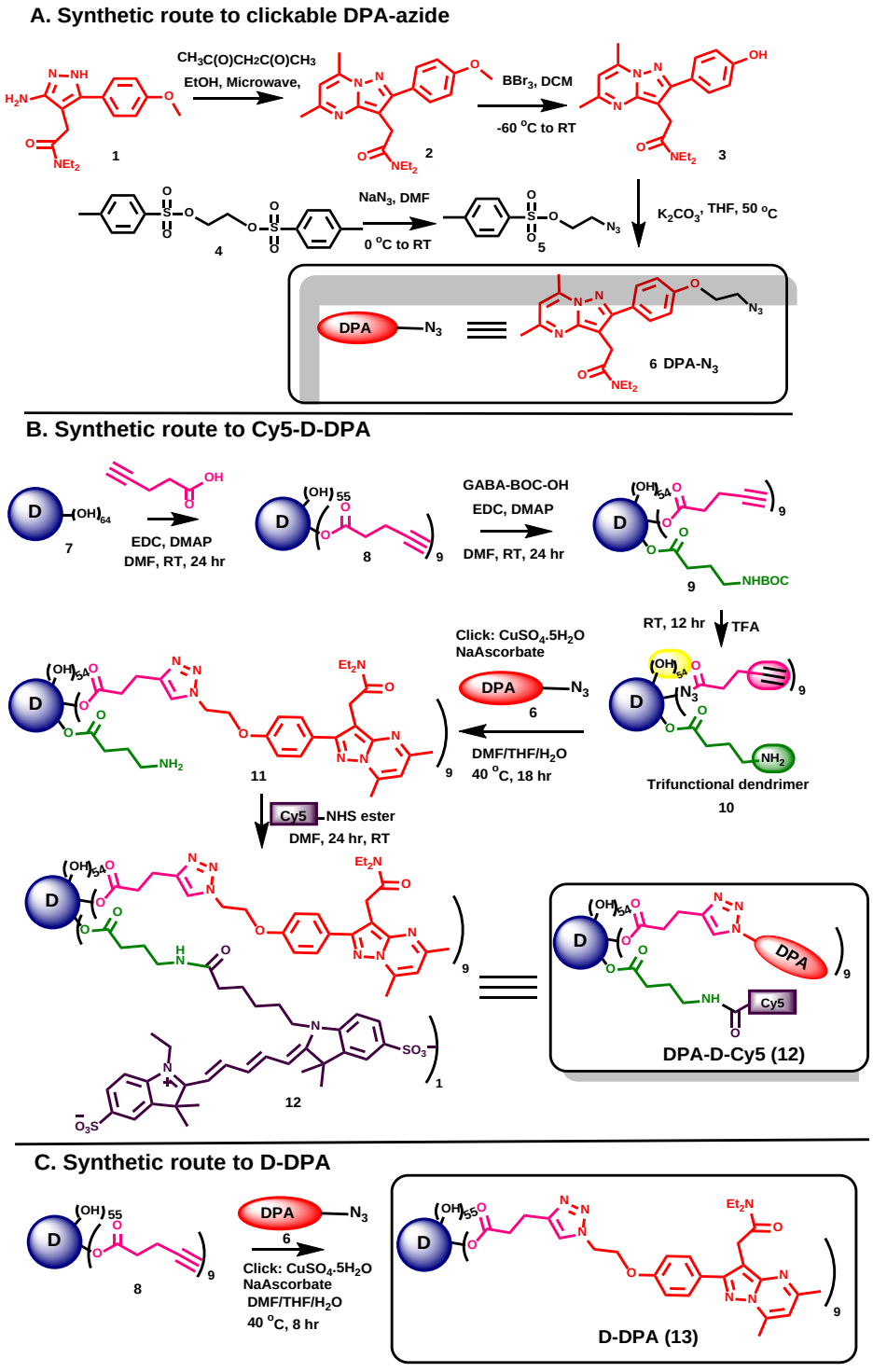

Figure 1. Synthesis of DPA derivative and dendrimer conjugates. Schematic representation of the synthesis pathways for **A)** conjugable azide-terminated DPA derivative (6, DPA-N_3), **B)** Cy5

fluorescently labelled dendrimer-DPA conjugate (12, Cy5-D-DPA), and **C)** dendrimer-DPA (13, D-DPA).

Chemical characterization of intermediates and final dendrimer-DPA conjugates

The structures of intermediates, DPA-triazole analogue, and the final dendrimer-DPA conjugates were characterized using ^{1}H NMR, mass spectroscopy and HPLC (**Figures S1-S21**). The ^{1}H NMR spectra of trifunctional dendrimer **10** (**Figure 2 A**, green spectrum) exhibited characteristic ester methylene protons from two linkers at δ 4.90 and 4.02 ppm. The comparative integration of protons from dendrimer internal amides at δ 8.19-7.64 ppm with ester methylene protons suggested the attachment of on an average ~9 alkyne linkers and ~2 amine terminating linkers. The success of the click reaction between DPA-azide and trifunctional dendrimer was analyzed via ^{1}H NMR by comparing the spectra of the resulting product (blue spectrum) with the starting materials (red and green spectra), showing the characteristic dendrimer peaks along with the DPA aromatic peaks in between δ 7.65-7.56, 7.00-6.90, and 6.77-6.71 ppm and aliphatic methyl protons at δ 1.10 and 0.93 ppm. Finally, the success of cy5 conjugation was evident from the Cy5 protons in the aromatic region (*magenta spectrum*). The purities of the final conjugates (D-DPA and Cy5-D-DPA) were >99% as analyzed by HPLC (**Figure 2B, Figures S17 and S19**). Conjugation of DPA to the dendrimer surface resulted in a shift in retention time from 19.9 minutes for trifunctional dendrimer to 23.1 minutes for Cy5-D-DPA (**Figure 2B**). DLS and zeta potential measurements revealed a hydrodynamic radius of 4.8 nm (**Figure 2C and D**) and ζ-potential of +3.6 mV (**Figure 2D and E**).

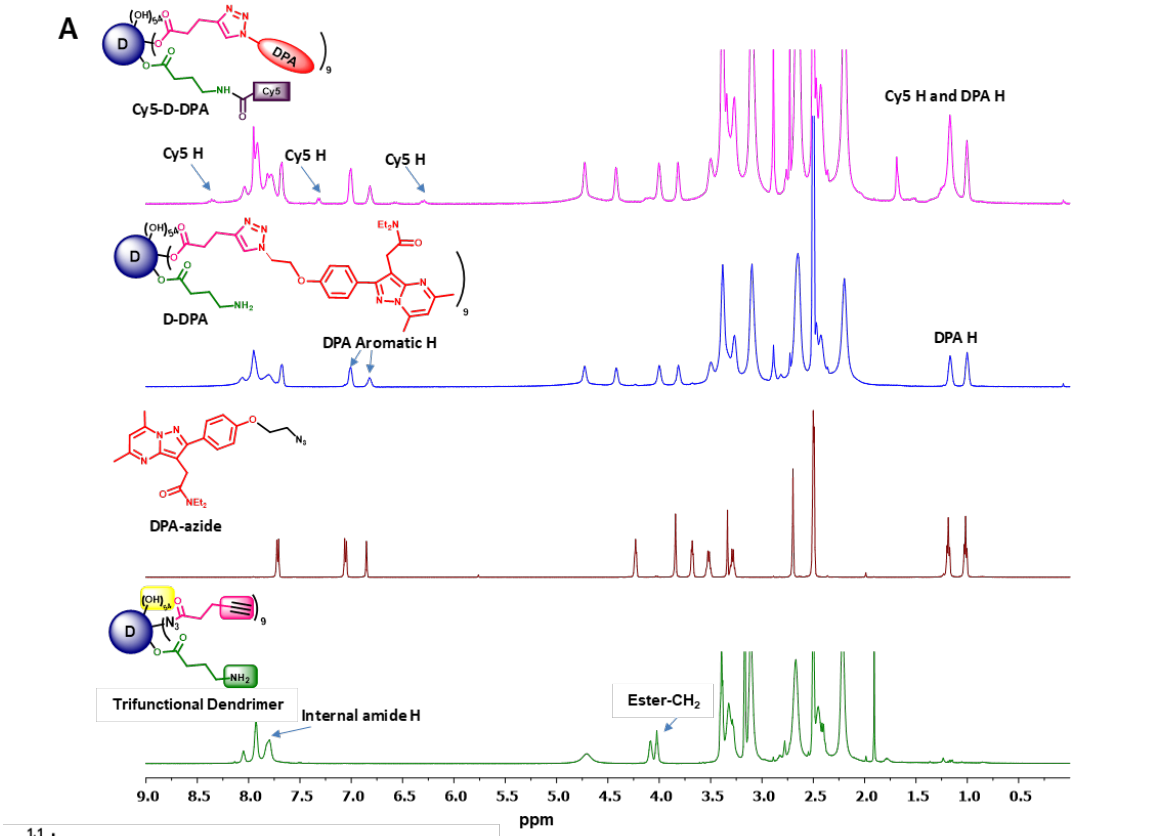

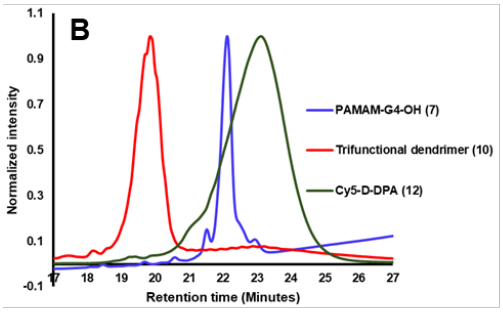

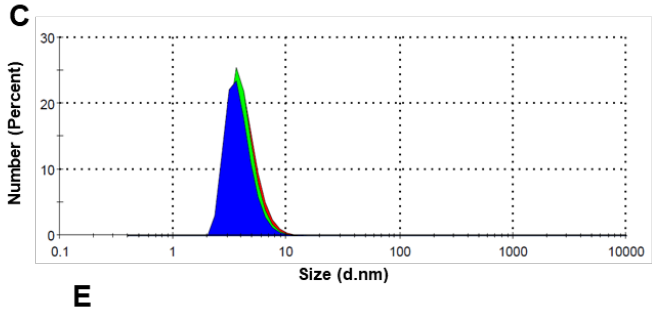

D

Sr. No.	Characterization	Result
1.	Size	4.8 ± 0.4 nm
2.	Zeta potential	+3.6 ± 0.6 mV
3.	Number of DPA molecules per dendrimer	~9
4.	HPLC purity	>99%
5.	Molecular weight	18.7 kDa

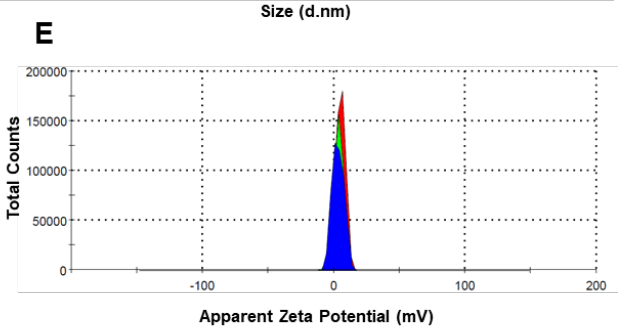

Figure 2. Chemical characterization of intermediate products and final conjugates. A) Comparative ^{1}H NMR spectra of fluorescently labelled dendrimer-DPA conjugate (Cy5-D-DPA), dendrimer-DPA (D-DPA), DPA-azide, and trifunctional dendrimer. Characteristic proton

signals are labelled. **B)** Comparative HPLC chromatogram of intermediates and final conjugate. **C)** Size distribution of D-DPA measured using dynamic light scattering (DLS). **D)** A table showing physicochemical characterization of D-DPA. **E)** Zeta potential distribution of D-DPA measured by DLS.

TSPO binding affinity of dendrimer-DPA conjugates

To evaluate whether D-DPA was active as a TSPO ligand, TSPO binding affinity in mitochondria was measured for D-DPA and was compared to free PK11195, DPA-triazole, and empty dendrimer (D-OH) (**Table 1**). The half-maximal inhibitory concentration (IC_{50}) of D-DPA was 70nM +/- 4, approximately 14-fold less potent relative to free PK11195 (5nM +/- 0.5) and ~1.4-fold more potent than the DPA-triazole analogue (100nM+/-20). The negative control empty dendrimer (D-OH) displayed no binding affinity.

Table 1. Comparative half-maximal inhibitory concentration (IC_{50}) of PK11195, DPA-triazole monomer, D-DPA and PAMAM-D-OH affinity to TSPO receptor.

Compound	Structure	Average IC_{50}
PK11195 (F wt. 353 Da)	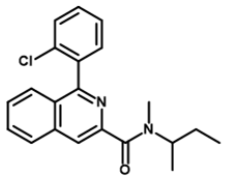	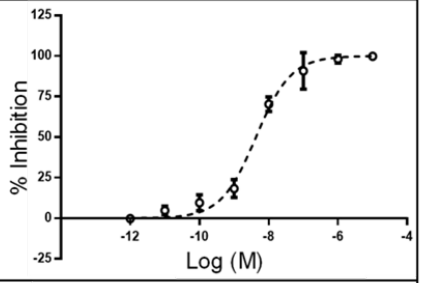
DPA-triazole (F. wt. 478 Da)	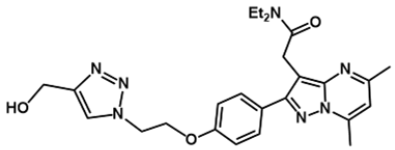	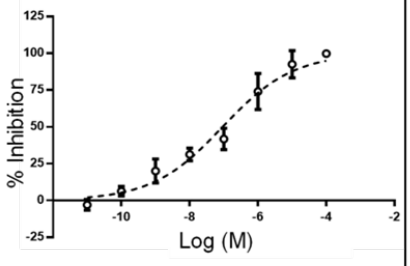
D-DPA (F. wt. 18.7 kDa)	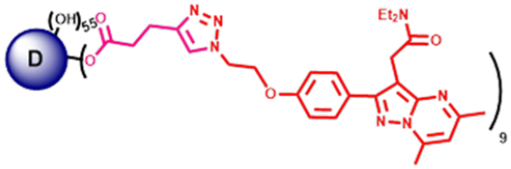	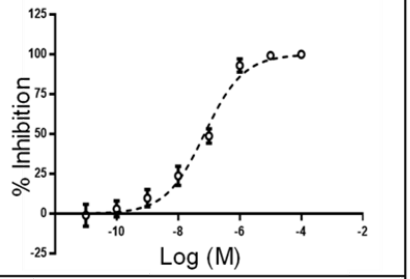
D-OH (F. wt. 14.3 kDa)	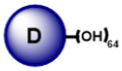	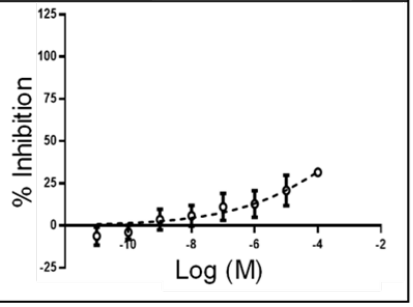

DPA conjugation to dendrimer enables mitochondrial targeting

Before proceeding with *in vitro* experiments, we first assessed the potential cytotoxicity of PK11195 and D-DPA via cell viability measurements. BV2 murine microglia were exposed to PK11195 or D-DPA over a concentration range of 1-1000 µg/mL for 24 hours. Consistent with

previous *in vitro* studies,[43, 44] PK11195 demonstrated significant dose-dependent toxicity, with the 1000 µg/mL dose reducing cell viability to ~5% of controls (**Figure S22**). In contrast, D-DPA exhibited significantly less cytotoxicity ($p < 0.0001$ PK11195 vs. D-DPA), with the 1000 µg/mL dose exhibiting ~60% cell viability. PK11195 has been shown to induce apoptosis via interference with mitochondrial permeability pores, so the slightly weaker binding affinity by D-DPA may contribute to the significantly reduced cytotoxicity.[45] This indicates that dendrimer delivery of a TSPO ligand may ameliorate cytotoxic effects for more effective and safer therapies.

Previous *in vivo* dendrimer work has shown that dendrimers selectively target TAMs in gliomas.[33] To explore the mitochondria targeting capabilities of DPA-conjugated dendrimers, HMC3 human macrophages were exposed to Cy5-D-DPA for 48 hours at 50 µg/mL. Cells were then fixed and stained to label nuclei, cell membranes, and mitochondria. Cy5-D-DPA exhibited highly punctated signal corresponding to the mitochondria, as shown by the yellow signal indicating overlap between dendrimer (red) and mitochondria (green) signals (**Figure 3A**). In contrast, unmodified dendrimer (D-Cy5) exhibits diffuse perinuclear signal consistent with what we have observed previously *in vitro* and *in vivo*.[46] While some overlap between dendrimer and mitochondrial signal is observed with D-Cy5, this appears to arise from the broad, cytosolic signal pattern of D-Cy5 rather than specific interactions with mitochondria. Representative fluorescence line profiles through cells show that dendrimer and mitochondria signal correlate closely with Cy5-D-DPA, whereas D-Cy5 exhibits regions of mitochondrial signal without corresponding dendrimer signal and vice versa (**Figure 3B**). Semi-quantitative analysis shows that conjugation of DPA to the dendrimer increases its colocalization coefficient by ~2-fold (**Figure 3C**, $p < 0.0001$).

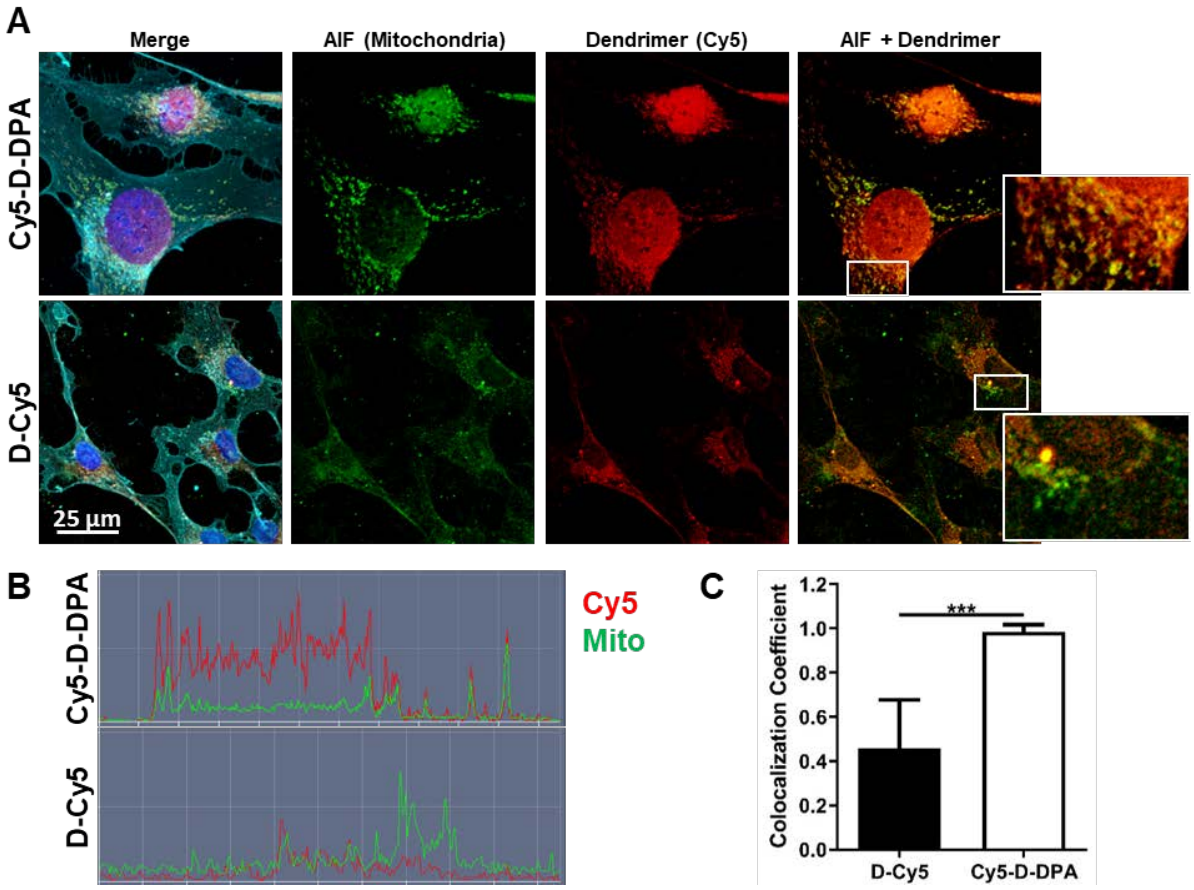

Figure 3. Conjugation of DPA to dendrimers enables targeting of mitochondria. HMC3 human macrophages were treated with fluorescently labelled dendrimer (red) with (Cy5-D-DPA) or without (D-Cy5) DPA conjugation. Following 48 hours of exposure cells were fixed and stained with DAPI to label cell nuclei (blue) and AIF to label mitochondria (green) for confocal imaging. **A)** Conjugation of DPA to dendrimers improves mitochondrial localization, as indicated by the yellow regions signifying colocalization of the green mitochondria and red dendrimer signal. D-Cy5 exhibits diffuse perinuclear signal. **B)** Representative fluorescence line profiles through cells demonstrates the close association between Cy5-D-DPA and mitochondrial signal, whereas D-Cy5 signal does not exhibit such correspondence. C) Cy5-D-DPA exhibits significantly greater colocalization coefficient with mitochondrial signal than D-Cy5. *** $p < 0.001$.

To further explore the mitochondria targeting properties of D-DPA, BV2 murine microglia were treated with unmodified or DPA-conjugated dendrimers for 24 hours. BV2 microglia were chosen due to their higher yield of isolated mitochondria compared to HMC3 macrophages. Cells were then fractionated to yield mitochondrial and cytosolic fractions. Cy5-D-DPA exhibited significantly greater partitioning to the isolated mitochondrial fraction compared to D-Cy5 (**Figure S23A**, $p = 0.0021$). However, total cellular internalization was not changed (**Figure S23B**, $p = 0.859$), indicating that dendrimer uptake properties were preserved with DPA conjugation, consistent with previous studies where up to 20 wt% loading of conjugated therapies did not interfere with dendrimer interactions with cells.[47]

Dendrimer-DPA promotes anti-tumor immune signaling

To evaluate the impact of PK11195 or D-DPA treatment on modulating TAMs-like phenotype, markers of immune activation were assessed after treatment in LPS stimulated BV2 murine microglia. LPS was chosen due to its role in promoting tumor immune recruitment, metastasis, and proliferation.[48] D-DPA treatment (100 μg/mL on a DPA loading basis) significantly increased secretions of TNFα by activated microglia ~2-fold compared to PK11195 treatment (100 μg/mL) (**Figure 4A**). D-DPA treatment similarly upregulated expression of anti-tumor, pro-inflammatory cytokines TNFα and IL1β ~3-fold compared to PK11195 treatment (**Figure 4C and D**). Notably, both PK11195 and D-DPA treatment did not upregulate anti-inflammatory signal Arg-1 (**Figure 4E**). Both PK11195 and D-DPA did decrease secretion of reactive oxygen species (**Figure 4B**), which are implicated in tumor recruitment of TAMs, tumorigenesis via inducing DNA damage, and tumor proliferation.[49, 50] These results indicate that in the context of TAMs-like immune activation, D-DPA exerts TSPO agonism activity to promote pro-inflammatory, anti-tumor immune signaling while reducing oxidative stress.

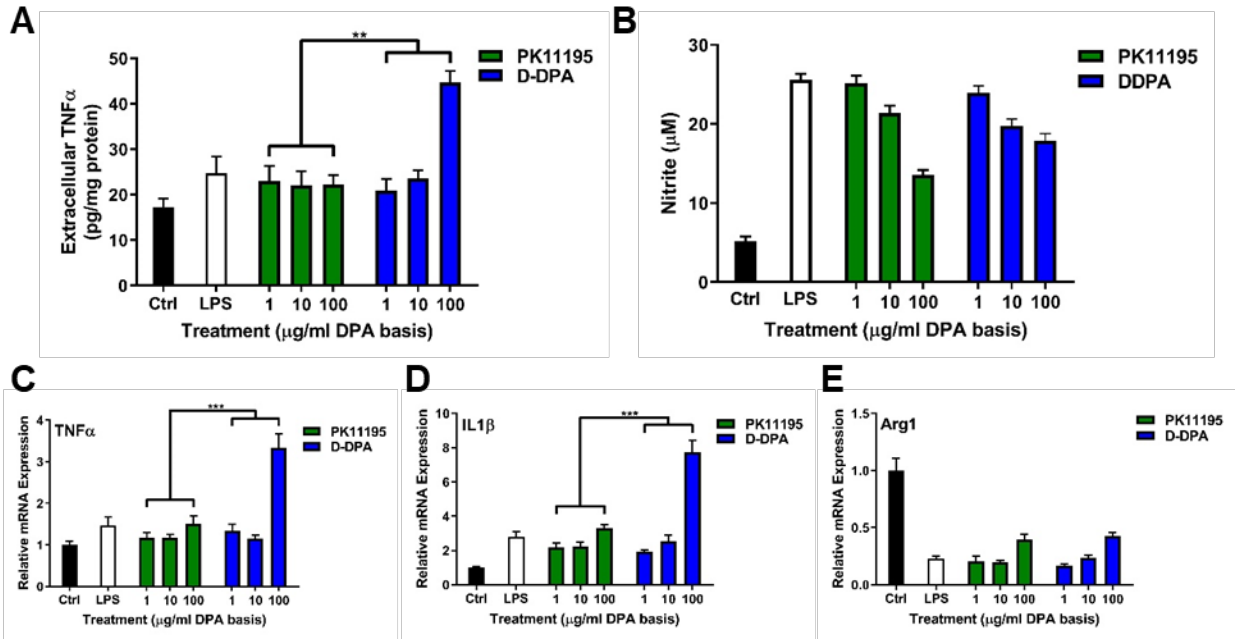

Figure 4. D-DPA treatment increases anti-tumor inflammatory signals. BV2 murine microglia were stimulated with LPS at 300 EU/mL for 3 hours, followed by cotreatment with PK11195 or DPA-conjugated dendrimer (D-DPA) for 24 hours. Then, cells were exposed to fresh media for 24 hours and collected for analyses of cellular and extracellular signals. **A)** Treatment with D-DPA significantly increases the secretion of TNFα, a tumor-killing signal, from stimulated BV2 microglia compared to PK11195 treatment. ** $p < 0.01$. **B)** Both treatments reduced secretion of nitrite, a reactive oxygen species indicative of oxidative stress. Analyses of mRNA expression via rt-qPCR demonstrates that D-DPA significantly increases expression of anti-tumor signals **C)** TNFα and **D)** IL1β while limiting expression of **E)** pro-tumor cytokine arginase-1 (Arg1). *** $p < 0.001$.

Systemically administered dendrimer-DPA targets mitochondria specifically within TAMs in vivo

Based on these promising *in vitro* results, we proceeded to evaluate *in vivo* targeting properties of the dendrimer-DPA conjugate in an orthotopic, immunocompetent model of

glioblastoma. First, to validate the rationale for TSPO targeting in this model of glioblastoma, we compared expression of TSPO within and outside the brain tumor. TSPO was significantly upregulated in the tumor ~5-fold compared to the contralateral hemisphere (**Figure S24**, $p < 0.0001$). In addition, we also examined the systemic biodistribution of Cy5-D-DPA compared to unmodified D-Cy5. TSPO has been shown to exhibit high expression in kidneys, livers, and spleens,[20, 51] creating the potential for off-target Cy5-D-DPA accumulation. Organs were collected 24 hours after systemic injection, and dendrimers were extracted and quantified using fluorescence spectrometry. Cy5-D-DPA exhibited similar levels in kidney, liver, and spleen compared to D-Cy5 (**Figure S25**). This indicates that Cy5-D-DPA is not interacting with TSPO expressed in peripheral organs for increased accumulation. Therefore, the dendrimer transport properties dominate, and DPA interactions with TSPO arise only once dendrimers have carried DPA into the intracellular space.

Cy5-D-DPA was intravenously injected into mice with orthotopic glioblastoma brain tumors 14 days after tumor inoculation. Brains were collected 24 hours after injection, fixed, and stained for confocal imaging. Imaging in the tumor core indicated that Cy5-D-DPA fully penetrated the solid brain tumor upon systemic administration and targeted mitochondria within the tumor (**Figure 5**, white arrows). This signal contrasts with our previously observed diffuse, cytosolic signal pattern *in vivo* in TAMs of unmodified dendrimers, indicating that the addition of TSPO ligand DPA confers mitochondrial targeting.[38] Unlike in the *in vitro* images, nuclear targeting of Cy5-D-DPA was not observed. Notably, green signal corresponding to mitochondria were observed throughout the tumor, but Cy5-D-DPA only exhibited cellular signal in specific cells.

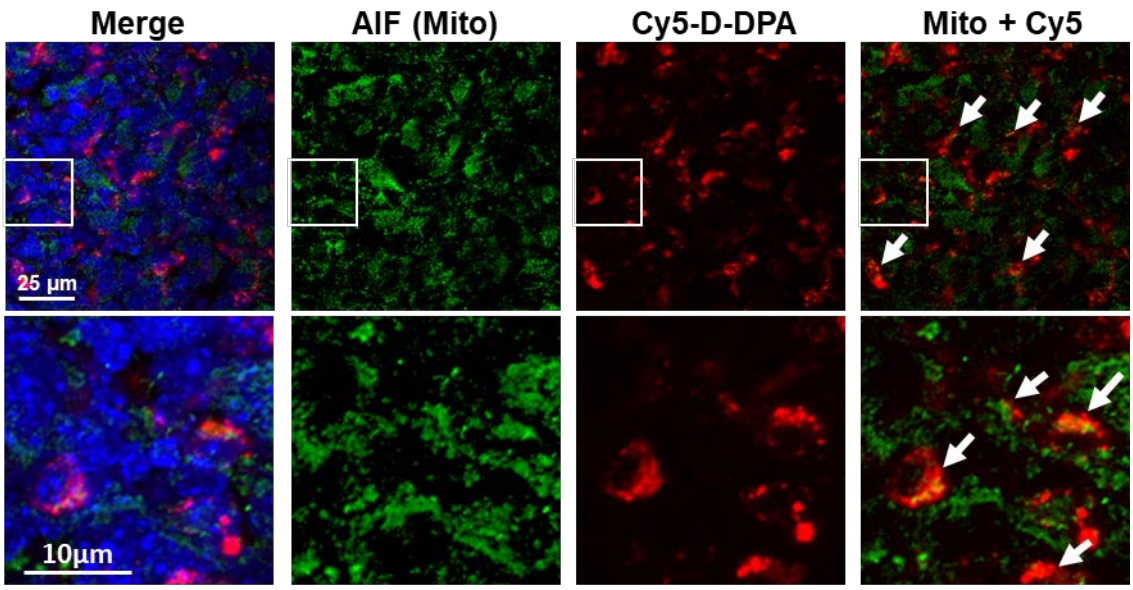

Figure 5. D-DPA targets mitochondria within the glioblastoma tumor. Glioblastoma brain tumor-bearing mice were injected intravenously with fluorescently labelled dendrimer-DPA conjugates (Cy5-D-DPA, red) 14 days after tumor inoculation. 24 hours after injection, brains were collected, fixed, and stained with DAPI to label cell nuclei (blue) and AIF to label mitochondria (Mito, green). Cy5-D-DPA targets mitochondria within the tumor (white arrows) in tumor-associated macrophages upon systemic administration. Localization with the nucleus as seen in the *in vitro* images was not observed *in vivo*.

To examine the cell type localization, we then stained brains with Iba1 to label TAMs. We observed that Cy5-D-DPA penetrated the solid tumor and distributed uniformly throughout, with high fidelity for the tumor border (**Figure 6A**). Minimal Cy5-D-DPA signal was observed in the surrounding healthy tissue, indicating highly specific tumor targeting. Imaging at higher magnification revealed that dendrimer signal was within TAMs (**Figure 6B**, white arrows). Therefore, DPA-conjugated dendrimers localize specifically to TAMs and target their mitochondria.

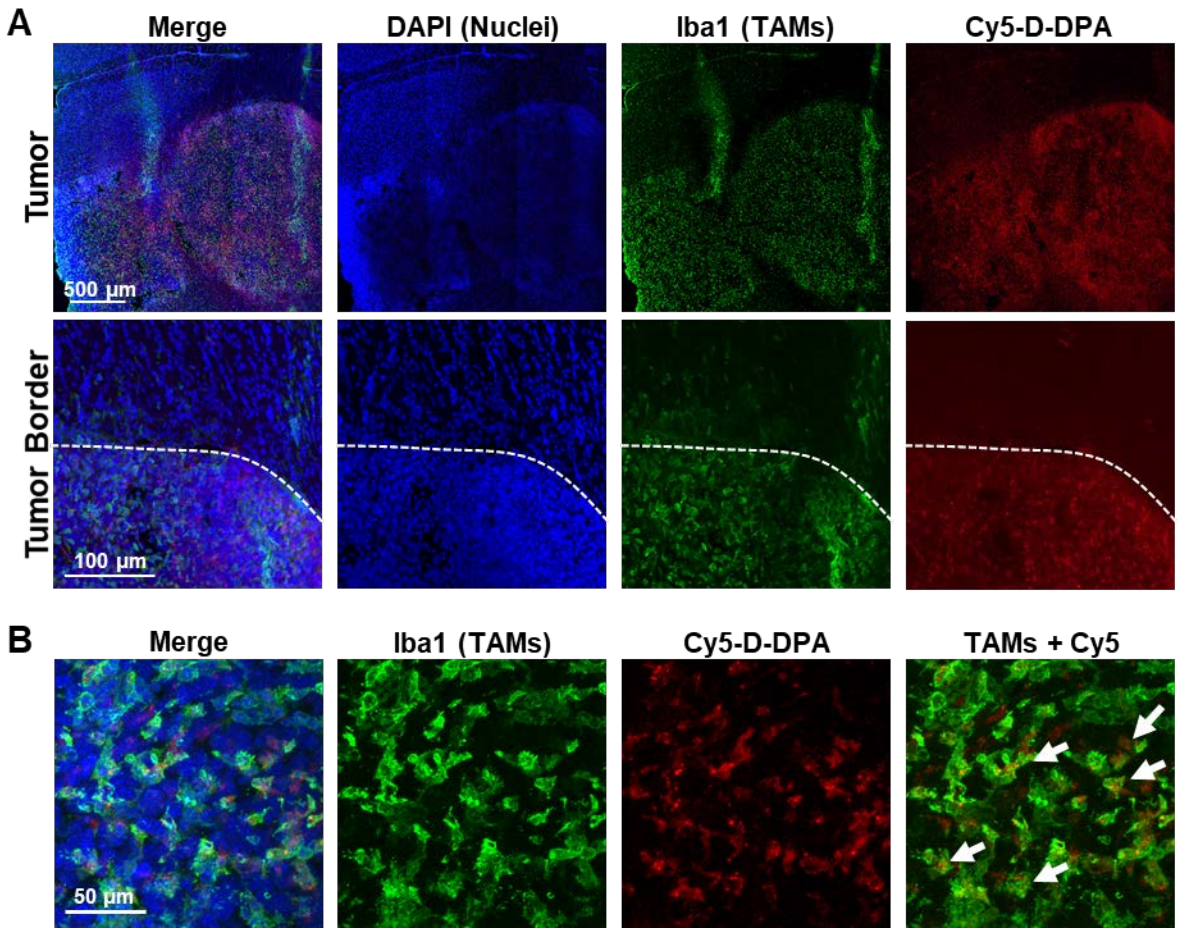

Figure 6. D-DPA specifically localizes to tumor-associated macrophages in the glioblastoma tumor upon systemic administration. Glioblastoma brain tumor-bearing mice were injected intravenously with fluorescently labelled dendrimer-DPA conjugates (Cy5-D-DPA, red) 14 days after tumor inoculation. 24 hours after injection, brains were collected, fixed, and stained with DAPI to label cell nuclei (blue) and Iba1 to label tumor-associated macrophages (TAMs, green) for confocal imaging. **A)** Whole tumor images (top panels) demonstrate that Cy5-D-DPA penetrates throughout the solid glioblastoma tumor after systemic administration. Imaging of the tumor border (bottom panels) demonstrate that Cy5-D-DPA localizes specifically within the tumor with high fidelity for the tumor border. **B)** Cy5-D-DPA signal colocalizes with Iba1 (white arrows), indicating specific targeting of TAMs within the glioblastoma tumor.

Discussion

In this study, we present a novel TSPO targeting generation 4 hydroxyl terminated PAMAM dendrimer by conjugating DPA targeting ligands to the dendrimer surface. Upon systemic administration, the dendrimer conjugate penetrates and distributes homogeneously within the solid GBM tumor with high specificity compared to healthy brain tissue. The surface decoration with DPA enables specific targeting of mitochondria within TAMs. *In vitro*, we demonstrate that by using the dendrimer conjugate to target TSPO, we can induce anti-tumor immune signaling to potentially promote the tumor-killing immune response.

DPA was conjugated to the surface of the dendrimer through copper catalyzed click reaction. This method of copper catalyzed click was utilized as the conjugation chemistry due to its robust and highly efficient chemistry. In addition, previous reports have shown that modification of the side chain of DPA with a phenethyl ring achieved the most effective binding affinity.[27] By utilizing this click chemistry approach, a triazole ring was introduced with ethyl spacer. We hypothesized that by mimicking this aromatic ring shown to enhance binding affinity to TSPO, optimal binding affinity of DPA on the dendrimer could be achieved. To assess binding affinity to TSPO, mitochondria were isolated from adrenal tissues. PK11195 exhibited 5 nM binding affinity to TSPO, consistent with previous reports (**Table 1**).[27] As expected, unmodified dendrimer exhibited no binding affinity for TSPO, as shown by the >100,000 nM IC_{50}. Dendrimer-DPA conjugates (D-DPA) exhibited an average IC_{50} of 70 nM. While we had expected binding affinity to improved compared to PK11195or DPA-triazole monomer due to multivalency effects.[52] D-DPA only showed slight improvement to DPA-triazole monomer. DPA moieties may be scattered across the dendrimer surface to prevent simultaneous presentation of multiple ligands to the TSPO receptor. However, the ~1.4-fold enhanced binding affinity

exhibited by D-DPA compared to DPA-triazole is consistent with some reports where conjugation of ligands yields unchanged or decreased binding affinity for their target due to attachment to bulky macromolecules which can interfere with receptor interactions.[53, 54] However, the compromised binding affinity as compared to free TSPO ligand (PK11195) can be overcome by inherent TAM targeting potential of dendrimers *in vivo*.

While nanoparticle-mediated strategies have extensively explored cell-type specific targeting, the development of enhanced nanoparticles displaying targeting ligands to achieve intracellular targeting in addition to cell-specific targeting remains an incredibly promising and relatively little explored space. In particular, mitochondria within activated immune cells, such as TAMs in the context of cancers, are attractive therapeutic targets due to their roles in regulating the tumor immune response. The mitochondrial colocalization of Cy5-D-DPA compares favorably to other nanoparticle platforms targeting mitochondria, which exhibit colocalization of 40-60%.[55, 56] Notably, the colocalization of Cy5-D-DPA also compared favorably to TPP-conjugated PAMAM dendrimers, which exhibit colocalization with mitochondria of ~65%.[41] This indicates that receptor-mediated mitochondrial targeting may yield more effective targeting compared to electrostatic-mediated strategies. These results demonstrate that these hydroxyl PAMAM dendrimers are promising vehicles for intracellular delivery, and they can be further modified to effectively target intracellular compartments such as the mitochondria. Notably, while previous studies have not explored this mitochondrial targeting *in vivo*, while we demonstrate that Cy5-D-DPA specifically targets mitochondria within TAMs following systemic administration.

Interestingly, D-DPA exhibited robust localization with the nucleus *in vitro* which has not been observed previously with these dendrimers. This phenomenon may arise from the role

of TSPO in mediating mitochondria-nuclear signaling.[57] TSPO upregulation has also been shown to occur in the context of inflammation on other membrane-bound organelles,[58] so D-DPA may be targeting TSPO expressed on the nuclear membrane. However, *in vivo* we did not observe nuclear targeting with D-DPA in the GBM tumor. This nuclear targeting property is beyond the scope of this study but warrants further exploration and may inform delivery for genetic material or therapies that target nuclear-localized factors.

TSPO targeting has been shown to influence immune activation, although its effects have shown conflicting results. Some studies have reported anti-inflammatory neuroprotective activity of PK11195,[59, 60] while others have shown that PK11195 exacerbates neurodegeneration and promotes apoptosis.[61, 62] This differential activity appears to depend on PK11195 activity as an agonist or antagonist of TSPO in specific disease contexts. Here, we show that D-DPA significantly upregulates anti-tumor signaling of TNFα and IL1β, as well as limits the expression of pro-tumor signal Arg-1 (**Figure 4**). This is consistent with previous reports where TSPO ligands can induce expression of TNFα and other pro-inflammatory cytokines.[63, 64] Due to the slightly weaker binding affinity of D-DPA for TSPO compared to PK11195, this improvement in promoting anti-tumor signaling is likely attributable to the high levels of cellular internalization exhibited by these dendrimers.[65] This has promising implications for cancer therapy, since delivery of gene vectors encoding TNFα or direct administration of TNFα have been shown to inhibit tumor progression.[66] Interestingly, PK11195 has been shown to exacerbate TNFα-induced apoptosis, which may contribute to its dose-dependent cytotoxicity (**Figure S22**). However, despite significantly increasing the induced expression levels of TNFα, D-DPA does not demonstrate the associated TNFα-induced cell death. This may be due to weaker interactions with TSPO due its binding affinity, although the precise mechanism of how D-DPA seems to

decouple promotion of TNFα expression from TNFα-induced apoptosis warrants further investigation. Both PK11195 and D-DPA reduced secretion of nitric oxide, consistent with previous reports where PK11195 treatment ameliorates ROS production.[67] These findings have exciting implications for glioblastoma treatment, as dendrimer presentation of the targeting ligand alone elicits anti-tumor immune activation *in vitro* and can be coupled with dendrimer delivery of mitochondria-targeted therapeutics for multi-modal synergistic effects.

Interestingly, we observed a small amount of dendrimer signal outside TAMs, and the morphology of these signals suggest that they reside within cells. Recent studies in interactions between tumor cells and immune cells have revealed that whole mitochondria may be transferred between cells.[68] Metabolic shifts in cancer cells leads them to generate energy via glycolysis rather than mitochondrial respiration, and highly glycolytic cancer cells correlate with poor patient outcomes.[69] However, cancer cells exhibiting respiratory incompetence are also deficient in other tumor progression functions and communicate with surrounding cells such as stromal cells and TAMs to acquire functional mitochondria to compensate.[69] Therefore, the small amount of signal observed outside TAMs may arise from Cy5-D-DPA being transferred to cancer cells along with mitochondria. The reasons and mechanisms behind this emerging concept require further exploration but may have significant implications for mitochondrial-targeted immunotherapies.

Conclusion

In this study, we present the design and synthesis of a DPA-conjugated dendrimer for targeting of mitochondria in TAMs. Dendrimers surface decorated with DPA moieties exhibited strong binding to TSPO, favorable *in vivo* TAMs targeting, and cellular internalization. We demonstrate that DPA-conjugated dendrimers exhibit significantly greater colocalization with

mitochondria compared to unmodified dendrimers. By targeting TSPO, the DPA-conjugated dendrimers stimulate anti-tumor immune signaling superior to PK11195, a classical TSPO ligand. *In vivo*, systemically administered dendrimer-DPA penetrate the solid brain tumor with high specificity and localized within TAMs to target mitochondria on a cell-type specific level. These results suggest that dendrimer-DPA may significantly improve targeted delivery of immunotherapies to mitochondria specifically within TAMs for the treatment of glioblastoma and other cancers.

Supporting Information

The characterization including NMR, mass spectra and HPLC chromatogram and the supporting biology figures are available in supporting information file.

Acknowledgements

This study was funded by the NIBIB R01EB01 8306 (RM Kannan), and NINDS 5R01NS093416 (SK, RMK and BS). We kindly thank the Wilmer Core Grant for Vision, Research, Microscopy, and Imaging Core Module (Grant #EY001865) for access to the Leica CM 1905 cryostat and Zen LSN710 confocal microscope.

Conflicts of Interest

The authors (RMK, SK, BS, RS, AS) have pending, awarded and licensed patents relating to the microglia and tumor-associated macrophage targeting and therapeutic hydroxyl PAMAM dendrimer platforms. RMK and SK are co-founders, have financial interests in Ashvattha Therapeutics LLC, Orpheris Inc., and RiniSight, three startups involved with the translation of dendrimer drug delivery platforms. RMK, SK and BS serve as Board of Directors of Ashvattha Therapeutics Inc.

Author contributions

A.S., K.L., R.S., S.K and R.M.K. conceptualized the experiments. A.S. and R.S. performed all synthesis and characterization of the dendrimer conjugates. K.L. performed the biological experiments. A.T. performed the binding studies. A.S. and K.L. wrote the manuscript, and A.S., K.L., A.T., B.S., and R.M.K edited the manuscript.

References

1. Myers, M. G., Moonlighting in Mitochondria. *Science* **2009,** 323, (5915), 723.
2. Heller, A.; Brockhoff, G.; Goepferich, A., Targeting drugs to mitochondria. *Eur J Pharm Biopharm* **2012,** 82, (1), 1-18.
3. Scatena, R., Mitochondria and cancer: a growing role in apoptosis, cancer cell metabolism and dedifferentiation. *Adv Exp Med Biol* **2012,** 942, 287-308.
4. Johri, A.; Beal, M. F., Mitochondrial dysfunction in neurodegenerative diseases. *J Pharmacol Exp Ther* **2012,** 342, (3), 619-630.
5. Sorrentino, V.; Menzies, K. J.; Auwerx, J., Repairing Mitochondrial Dysfunction in Disease. *Annu Rev Pharmacol Toxicol* **2018,** 58, 353-389.
6. Ksiezakowska-Lakoma, K.; Zyla, M.; Wilczynski, J. R., Mitochondrial dysfunction in cancer. *Prz Menopauzalny* **2014,** 13, (2), 136-44.
7. Fulda, S.; Galluzzi, L.; Kroemer, G., Targeting mitochondria for cancer therapy. *Nat. Rev. Drug Discov.* **2010,** 9, (6), 447-464.
8. Pustylnikov, S.; Costabile, F.; Beghi, S.; Facciabene, A., Targeting mitochondria in cancer: current concepts and immunotherapy approaches. *Transl Res* **2018,** 202, 35-51.
9. Buck, M. D.; O'Sullivan, D.; Klein Geltink, R. I.; Curtis, J. D.; Chang, C. H.; Sanin, D. E.; Qiu, J.; Kretz, O.; Braas, D.; van der Windt, G. J.; Chen, Q.; Huang, S. C.; O'Neill, C. M.; Edelson, B. T.; Pearce, E. J.; Sesaki, H.; Huber, T. B.; Rambold, A. S.; Pearce, E. L., Mitochondrial Dynamics Controls T Cell Fate through Metabolic Programming. *Cell* **2016,** 166, (1), 63-76.
10. Scharping, N. E.; Menk, A. V.; Moreci, R. S.; Whetstone, R. D.; Dadey, R. E.; Watkins, S. C.; Ferris, R. L.; Delgoffe, G. M., The Tumor Microenvironment Represses T Cell Mitochondrial Biogenesis to Drive Intratumoral T Cell Metabolic Insufficiency and Dysfunction. *Immunity* **2016,** 45, (2), 374-88.
11. Pearce, E. L.; Pearce, E. J., Metabolic pathways in immune cell activation and quiescence. *Immunity* **2013,** 38, (4), 633-43.
12. Mills, E. L.; O'Neill, L. A., Reprogramming mitochondrial metabolism in macrophages as an anti-inflammatory signal. *Eur. J. Immunol.* **2016,** 46, (1), 13-21.
13. Liou, G.-Y.; Storz, P., Reactive oxygen species in cancer. *Free Radic Res* **2010,** 44, (5), 479-496.
14. Murphy, M. P., How mitochondria produce reactive oxygen species. *Biochem J* **2009,** 417, (1), 1-13.
15. Ostuni, M. A.; Issop, L.; Péranzi, G.; Walker, F.; Fasseu, M.; Elbim, C.; Papadopoulos, V.; Lacapere, J.-J., Overexpression of translocator protein in inflammatory bowel disease: potential diagnostic and treatment value. *Inflamm Bowel Dis* **2010,** 16, (9), 1476-1487.

16. Sambi, M.; Bagheri, L.; Szewczuk, M. R., Current Challenges in Cancer Immunotherapy: Multimodal Approaches to Improve Efficacy and Patient Response Rates. *J Oncol* **2019,** 2019, 4508794-4508794.
17. Cassetta, L.; Kitamura, T., Targeting Tumor-Associated Macrophages as a Potential Strategy to Enhance the Response to Immune Checkpoint Inhibitors. *Front Cell Dev Biol* **2018,** 6, 38-38.
18. Rupprecht, R.; Papadopoulos, V.; Rammes, G.; Baghai, T. C.; Fan, J.; Akula, N.; Groyer, G.; Adams, D.; Schumacher, M., Translocator protein (18 kDa) (TSPO) as a therapeutic target for neurological and psychiatric disorders. *Nat. Rev. Drug Discov.* **2010,** 9, (12), 971-988.
19. Batarseh, A.; Papadopoulos, V., Regulation of translocator protein 18 kDa (TSPO) expression in health and disease states. *Mol Cell Endocrinol* **2010,** 327, (1-2), 1-12.
20. Bhoola, N. H.; Mbita, Z.; Hull, R.; Dlamini, Z., Translocator Protein (TSPO) as a Potential Biomarker in Human Cancers. *Int J Mol Sci* **2018,** 19, (8), 2176.
21. Werry, E. L.; Barron, M. L.; Kassiou, M., TSPO as a target for glioblastoma therapeutics. *Biochem Soc Trans* **2015,** 43, (4), 531-6.
22. Roncaroli, F.; Su, Z.; Herholz, K.; Gerhard, A.; Turkheimer, F. E., TSPO expression in brain tumours: is TSPO a target for brain tumour imaging? *Clin Transl Imaging* **2016,** 4, 145-156.
23. Albert, N. L.; Unterrainer, M.; Fleischmann, D. F.; Lindner, S.; Vettermann, F.; Brunegraf, A.; Vomacka, L.; Brendel, M.; Wenter, V.; Wetzel, C.; Rupprecht, R.; Tonn, J. C.; Belka, C.; Bartenstein, P.; Niyazi, M., TSPO PET for glioma imaging using the novel ligand (18)F-GE-180: first results in patients with glioblastoma. *Eur J Nucl Med Mol Imaging* **2017,** 44, (13), 2230-2238.
24. Mukherjee, S.; Sonanini, D.; Maurer, A.; Daldrup-Link, H. E., The yin and yang of imaging tumor associated macrophages with PET and MRI. *Theranostics* **2019,** 9, (25), 7730-7748.
25. Azrad, M.; Zeineh, N.; Weizman, A.; Veenman, L.; Gavish, M., The TSPO Ligands 2-Cl-MGV-1, MGV-1, and PK11195 Differentially Suppress the Inflammatory Response of BV-2 Microglial Cell to LPS. *Int J Mol Sci* **2019,** 20, 594.
26. Wu, X.; Gallo, K. A., The 18-kDa Translocator Protein (TSPO) Disrupts Mammary Epithelial Morphogenesis and Promotes Breast Cancer Cell Migration. *PLOS ONE* **2013,** 8, (8), e71258.
27. Banister, S. D.; Beinat, C.; Wilkinson, S. M.; Shen, B.; Bartoli, C.; Selleri, S.; Da Pozzo, E.; Martini, C.; Chin, F. T.; Kassiou, M., Ether analogues of DPA-714 with subnanomolar affinity for the translocator protein (TSPO). *Eur J Med Chem* **2015,** 93, 392-400.
28. Hagens, M. H. J.; Golla, S. V.; Wijburg, M. T.; Yaqub, M.; Heijtel, D.; Steenwijk, M. D.; Schober, P.; Brevé, J. J. P.; Schuit, R. C.; Reekie, T. A.; Kassiou, M.; van Dam, A.-M.; Windhorst, A. D.; Killestein, J.; Barkhof, F.; van Berckel, B. N. M.; Lammertsma, A. A., In vivo assessment of neuroinflammation in progressive multiple sclerosis: a proof of concept study with [18F]DPA714 PET. *J. Neuroinflammation* **2018,** 15, (1), 314.
29. Banati, R. B.; Newcombe, J.; Gunn, R. N.; Cagnin, A.; Turkheimer, F.; Heppner, F.; Price, G.; Wegner, F.; Giovannoni, G.; Miller, D. H.; Perkin, G. D.; Smith, T.; Hewson, A. K.; Bydder, G.; Kreutzberg, G. W.; Jones, T.; Cuzner, M. L.; Myers, R., The peripheral benzodiazepine binding site in the brain in multiple sclerosis: Quantitative in vivo imaging of microglia as a measure of disease activity. *Brain* **2000,** 123, (11), 2321-2337.
30. Sharma, A.; Soliman, G. M.; Al-Hajaj, N.; Sharma, R.; Maysinger, D.; Kakkar, A., Design and Evaluation of Multifunctional Nanocarriers for Selective Delivery of Coenzyme Q10 to Mitochondria. *Biomacromolecules* **2012,** 13, (1), 239-252.
31. Lesniak, W. G.; Mishra, M. K.; Jyoti, A.; Balakrishnan, B.; Zhang, F.; Nance, E.; Romero, R.; Kannan, S.; Kannan, R. M., Biodistribution of fluorescently labeled PAMAM dendrimers in neonatal rabbits: effect of neuroinflammation. *Mol Pharm* **2013,** 10, (12), 4560-71.
32. Mishra, M. K.; Beaty, C. A.; Lesniak, W. G.; Kambhampati, S. P.; Zhang, F.; Wilson, M. A.; Blue, M. E.; Troncoso, J. C.; Kannan, S.; Johnston, M. V.; Baumgartner, W. A.; Kannan, R. M., Dendrimer Brain

Uptake and Targeted Therapy for Brain Injury in a Large Animal Model of Hypothermic Circulatory Arrest. *ACS Nano* **2014,** 8, (3), 2134-2147.
33. Zhang, F.; Mastorakos, P.; Mishra, M. K.; Mangraviti, A.; Hwang, L.; Zhou, J., Uniform brain tumor distribution and tumor associated macrophage targeting of systemically administered dendrimers. *Biomaterials* **2015,** 52.
34. Xiao, Y.; Shi, X., Improved tumor imaging using dendrimer-based nanoplatforms. *Nanomedicine* **2019,** 14, (19), 2515-2518.
35. Sharma, A.; Sharma, R.; Zhang, Z.; Liaw, K.; Kambhampati, S. P.; Porterfield, J. E.; Lin, K. C.; DeRidder, L. B.; Kannan, S.; Kannan, R. M., Dense hydroxyl polyethylene glycol dendrimer targets activated glia in multiple CNS disorders. *Sci. Adv.* **2020,** 6, (4), eaay8514.
36. Sharma, R.; Kambhampati, S. P.; Zhang, Z.; Sharma, A.; Chen, S.; Duh, E. I.; Kannan, S.; Tso, M. O. M.; Kannan, R. M., Dendrimer mediated targeted delivery of sinomenine for the treatment of acute neuroinflammation in traumatic brain injury. *J Control Release* **2020,** 323, 361-375.
37. Khoury, E. S.; Sharma, A.; Ramireddy, R. R.; Thomas, A. G.; Alt, J.; Fowler, A.; Rais, R.; Tsukamoto, T.; Blue, M. E.; Slusher, B.; Kannan, S.; Kannan, R. M., Dendrimer-conjugated glutaminase inhibitor selectively targets microglial glutaminase in a mouse model of Rett syndrome. *Theranostics* **2020,** 10, (13), 5736-5748.
38. Liaw, K.; Zhang, F.; Mangraviti, A.; Kannan, S.; Tyler, B.; Kannan, R. M., Dendrimer size effects on the selective brain tumor targeting in orthotopic tumor models upon systemic administration. *Bioeng Transl Med.* **2020,** 5, e10160.
39. Dobrovolskaia, M. A., Dendrimers Effects on the Immune System: Insights into Toxicity and Therapeutic Utility. *Curr Pharm Des* **2017,** 23, (21), 3134-3141.
40. Sharma, R.; Sharma, A.; Kambhampati, S. P.; Reddy, R. R.; Zhang, Z.; Cleland, J. L.; Kannan, S.; Kannan, R. M., Scalable synthesis and validation of PAMAM dendrimer-N-acetyl cysteine conjugate for potential translation. *Bioeng Transl Med* **2018,** 3, (2), 87-101.
41. Sharma, A.; Liaw, K.; Sharma, R.; Zhang, Z.; Kannan, S.; Kannan, R. M., Targeting Mitochondrial Dysfunction and Oxidative Stress in Activated Microglia using Dendrimer-Based Therapeutics. *Theranostics* **2018,** 8, (20), 5529-5547.
42. Sharma, A.; Porterfield, J. E.; Smith, E.; Sharma, R.; Kannan, S.; Kannan, R. M., Effect of mannose targeting of hydroxyl PAMAM dendrimers on cellular and organ biodistribution in a neonatal brain injury model. *J Control Release* **2018,** 283, 175-189.
43. Guedes, C. E. S.; Dias, B. R. S.; Petersen, A.; Cruz, K. P.; Almeida, N. J.; Andrade, D. R.; Menezes, J. P. B.; Borges, V. M.; Veras, P. S. T., In vitro evaluation of the anti-leishmanial activity and toxicity of PK11195. *Mem Inst Oswaldo Cruz* **2018,** 113, (4), e170345.
44. Fennell, D. A.; Corbo, M.; Pallaska, A.; Cotter, F. E., Bcl-2 resistant mitochondrial toxicity mediated by the isoquinoline carboxamide PK11195 involves de novo generation of reactive oxygen species. *Br. J. Cancer* **2001,** 84, (10), 1397-1404.
45. Mendonça-Torres, M. C.; Roberts, S. S., The translocator protein (TSPO) ligand PK11195 induces apoptosis and cell cycle arrest and sensitizes to chemotherapy treatment in pre- and post-relapse neuroblastoma cell lines. *Cancer Biol Ther* **2013,** 14, (4), 319-326.
46. Sharma, R.; Kim, S.-Y.; Sharma, A.; Zhang, Z.; Kambhampati, S. P.; Kannan, S.; Kannan, R. M., Activated Microglia Targeting Dendrimer–Minocycline Conjugate as Therapeutics for Neuroinflammation. *Bioconjugate Chem* **2017,** 28, (11), 2874-2886.
47. Nemeth, C. L.; Drummond, G. T.; Mishra, M. K.; Zhang, F.; Carr, P.; Garcia, M. S.; Doman, S.; Fatemi, A.; Johnston, M. V.; Kannan, R. M.; Kannan, S.; Wilson, M. A., Uptake of dendrimer-drug by different cell types in the hippocampus after hypoxic–ischemic insult in neonatal mice: Effects of injury, microglial activation and hypothermia. *Nanomed Nanotechnol* **2017,** 13, (7), 2359-2369.

48. Hsu, R. Y.; Chan, C. H.; Spicer, J. D.; Rousseau, M. C.; Giannias, B.; Rousseau, S.; Ferri, L. E., LPS-induced TLR4 signaling in human colorectal cancer cells increases beta1 integrin-mediated cell adhesion and liver metastasis. *Cancer Res* **2011,** 71, (5), 1989-98.
49. Reuter, S.; Gupta, S. C.; Chaturvedi, M. M.; Aggarwal, B. B., Oxidative stress, inflammation, and cancer: how are they linked? *Free Radic Biol Med* **2010,** 49, (11), 1603-1616.
50. Visconti, R.; Grieco, D., New insights on oxidative stress in cancer. *Curr Opin Drug Discov Devel* **2009,** 12, (2), 240-245.
51. Betlazar, C.; Harrison-Brown, M.; Middleton, R. J.; Banati, R.; Liu, G.-J., Cellular Sources and Regional Variations in the Expression of the Neuroinflammatory Marker Translocator Protein (TSPO) in the Normal Brain. *Int J Mol Sci* **2018,** 19, (9), 2707.
52. Kitov, P. I.; Bundle, D. R., On the Nature of the Multivalency Effect: A Thermodynamic Model. *J Am. Chem. Soc.* **2003,** 125, (52), 16271-16284.
53. Acchione, M.; Kwon, H.; Jochheim, C. M.; Atkins, W. M., Impact of linker and conjugation chemistry on antigen binding, Fc receptor binding and thermal stability of model antibody-drug conjugates. *MAbs* **2012,** 4, (3), 362-372.
54. Reichenwallner, J.; Thomas, A.; Steinbach, T.; Eisermann, J.; Schmelzer, C. E. H.; Wurm, F.; Hinderberger, D., Ligand-Binding Cooperativity Effects in Polymer–Protein Conjugation. *Biomacromolecules* **2019,** 20, (2), 1118-1131.
55. Kwon, H. J.; Cha, M.-Y.; Kim, D.; Kim, D. K.; Soh, M.; Shin, K.; Hyeon, T.; Mook-Jung, I., Mitochondria-Targeting Ceria Nanoparticles as Antioxidants for Alzheimer's Disease. *ACS Nano* **2016,** 10, (2), 2860-2870.
56. Yang, G.; Xu, L.; Xu, J.; Zhang, R.; Song, G.; Chao, Y.; Feng, L.; Han, F.; Dong, Z.; Li, B.; Liu, Z., Smart Nanoreactors for pH-Responsive Tumor Homing, Mitochondria-Targeting, and Enhanced Photodynamic-Immunotherapy of Cancer. *Nano Letters* **2018,** 18, (4), 2475-2484.
57. Yasin, N.; Veenman, L.; Singh, S.; Azrad, M.; Bode, J.; Vainshtein, A.; Caballero, B.; Marek, I.; Gavish, M., Classical and Novel TSPO Ligands for the Mitochondrial TSPO Can Modulate Nuclear Gene Expression: Implications for Mitochondrial Retrograde Signaling. *Int J Mol Sci* **2017,** 18, (4), 786.
58. Liu, G.-J.; Middleton, R. J.; Hatty, C. R.; Kam, W. W.-Y.; Chan, R.; Pham, T.; Harrison-Brown, M.; Dodson, E.; Veale, K.; Banati, R. B., The 18 kDa Translocator Protein, Microglia and Neuroinflammation. *Brain Pathol* **2014,** 24, (6), 631-653.
59. da Silva, M. B. S.; Farges, R. C.; Fröde, T. S., Involvement of steroids in anti-inflammatory effects of PK11195 in a murine model of pleurisy. *Mediators Inflamm* **2004,** 13, (2), 93-103.
60. Ryu, J. K.; Choi, H. B.; McLarnon, J. G., Peripheral benzodiazepine receptor ligand PK11195 reduces microglial activation and neuronal death in quinolinic acid-injected rat striatum. *Neurobiol Dis* **2005,** 20, (2), 550-561.
61. Papadopoulos, V.; Lecanu, L., Translocator protein (18 kDa) TSPO: An emerging therapeutic target in neurotrauma. *Exp. Neurol.* **2009,** 219, (1), 53-57.
62. Wu, Y.; Shamoto-Nagai, M.; Maruyama, W.; Osawa, T.; Naoi, M., Rasagiline prevents cyclosporine A-sensitive superoxide flashes induced by PK11195, the initial signal of mitochondrial membrane permeabilization and apoptosis. *J. Neural Transm.* **2016,** 123, (5), 491-494.
63. Lee, J.-W.; Nam, H.; Yu, S.-W., Systematic Analysis of Translocator Protein 18 kDa (TSPO) Ligands on Toll-like Receptors-mediated Pro-inflammatory Responses in Microglia and Astrocytes. *Exp Neurobiol* **2016,** 25, (5), 262-268.
64. Hatano, K.; Sekimata, K.; Yamada, T.; Abe, J.; Ito, K.; Ogawa, M.; Magata, Y.; Toyohara, J.; Ishiwata, K.; Biggio, G.; Serra, M.; Laquintana, V.; Denora, N.; Latrofa, A.; Trapani, G.; Liso, G.; Suzuki, H.; Sawada, M.; Nomura, M.; Toyama, H., Radiosynthesis and in vivo evaluation of two imidazopyridineacetamides, [11C]CB184 and [11C]CB190, as a PET tracer for 18 kDa translocator protein: direct comparison with [11C](R)-PK11195. *Ann. Nucl. Med.* **2015,** 29, (4), 325-335.

65. Liaw, K.; Gök, O.; DeRidder, L. B.; Kannan, S.; Kannan, R. M., Quantitative assessment of surface functionality effects on microglial uptake and retention of PAMAM dendrimers. *J Nanopart Res* **2018,** 20, (4), 111.
66. Lejeune, F. J.; Rüegg, C.; Liénard, D., Clinical applications of TNF-α in cancer. *Curr. Opin. Immunol.* **1998,** 10, (5), 573-580.
67. Issop, L.; Ostuni, M. A.; Lee, S.; Laforge, M.; Péranzi, G.; Rustin, P.; Benoist, J.-F.; Estaquier, J.; Papadopoulos, V.; Lacapère, J.-J., Translocator Protein-Mediated Stabilization of Mitochondrial Architecture during Inflammation Stress in Colonic Cells. *PloS one* **2016,** 11, (4), e0152919-e0152919.
68. Yang, D.; Kim, J., Mitochondrial Retrograde Signalling and Metabolic Alterations in the Tumour Microenvironment. *Cells* **2019,** 8, (3), 275.
69. Herst, P. M.; Dawson, R. H.; Berridge, M. V., Intercellular Communication in Tumor Biology: A Role for Mitochondrial Transfer. *Front Oncol* **2018,** 8, 344-344.

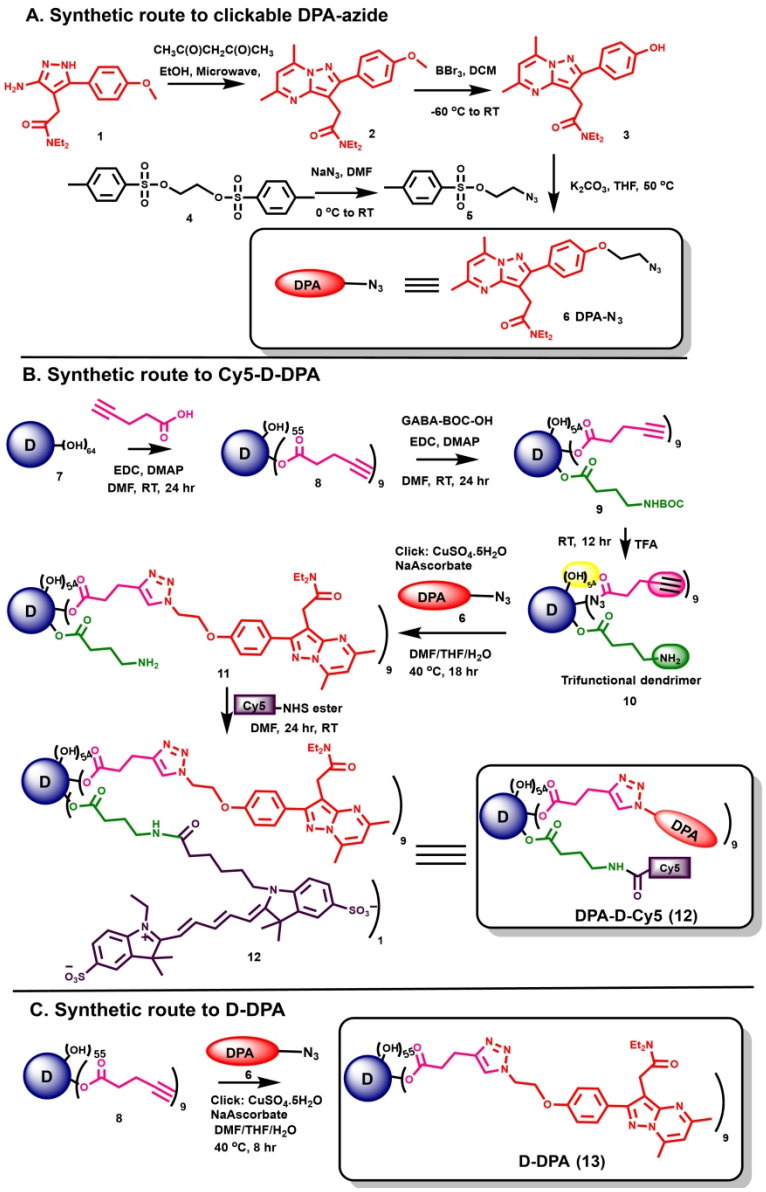

Figure 1. Synthesis of DPA derivative and dendrimer conjugates. Schematic representation of the synthesis pathways for A) conjugable azide-terminated DPA derivative (6, DPA-N3), B) Cy5 fluorescently labeled dendrimer-DPA conjugate (12, Cy5-D-DPA), and C) dendrimer-DPA (13, D-DPA).

558x846mm (144 x 144 DPI)

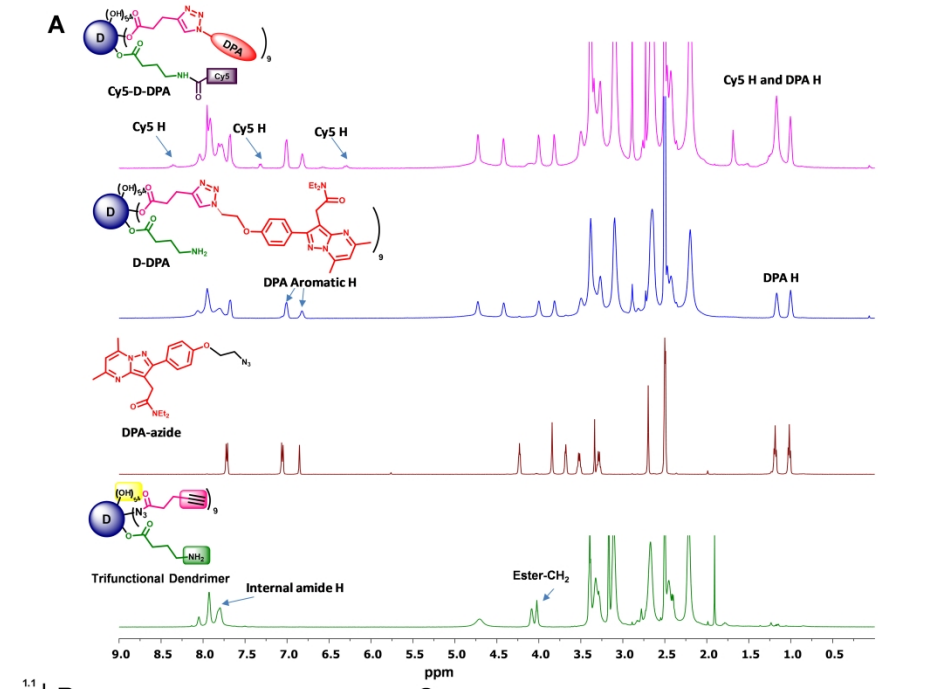

D

Sr. No.	Characterization	Result
1.	Size	4.8 ± 0.4 nm
2.	Zeta potential	+3.6 ± 0.6 mV
3.	Number of DPA molecules per dendrimer	~9
4.	HPLC purity	>99%
5.	Molecular weight	18.7 kDa

Figure 2. Chemical characterization of intermediate products and final conjugates. A) Comparative 1H NMR spectra of fluorescently labelled dendrimer-DPA conjugate (Cy5-D-DPA), dendrimer-DPA (D-DPA), DPA-azide, and trifunctional dendrimer. Characteristic proton signals are labelled. B) Comparative HPLC chromatogram of intermediates and final conjugate. C) Size distribution of D-DPA measured using dynamic light scattering (DLS). D) A table showing physicochemical characterization of D-DPA. E) Zeta potential distribution of D-DPA measured by DLS.

821x1010mm (144 x 144 DPI)

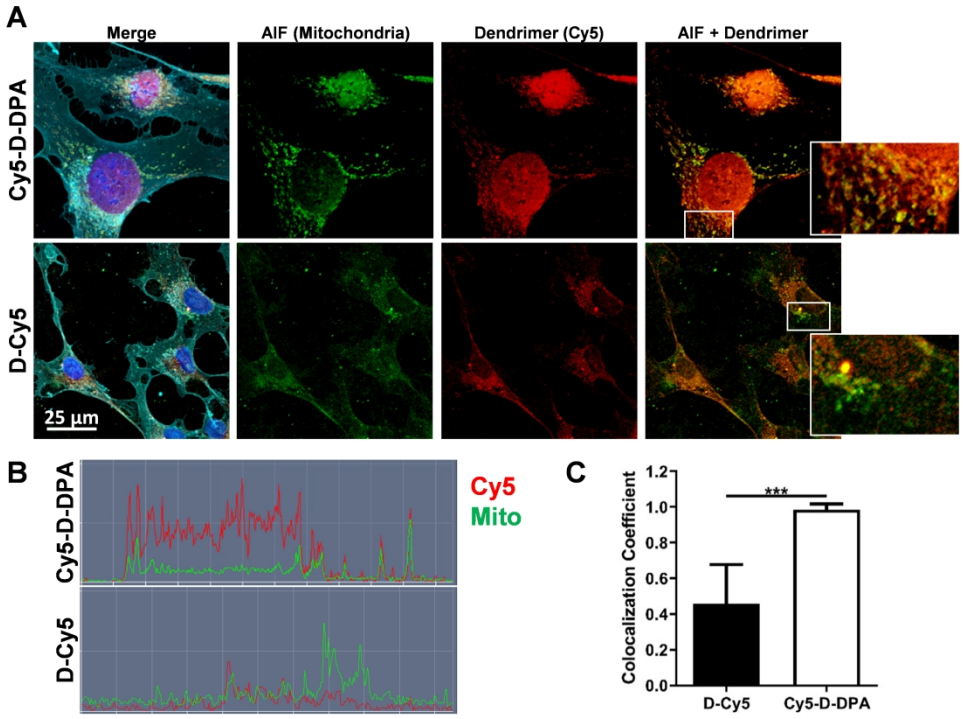

Figure 3. Conjugation of DPA to dendrimers enables targeting of mitochondria. HMC3 human macrophages were treated with fluorescently labelled dendrimer (red) with (Cy5-D-DPA) or without (D-Cy5) DPA conjugation. Following 48 hours of exposure cells were fixed and stained with DAPI to label cell nuclei (blue) and AIF to label mitochondria (green) for confocal imaging. A) Conjugation of DPA to dendrimers improves mitochondrial localization, as indicated by the yellow regions signifying colocalization of the green mitochondria and red dendrimer signal. D-Cy5 exhibits diffuse perinuclear signal. B) Representative fluorescence line profiles through cells demonstrates the close association between Cy5-D-DPA and mitochondrial signal, whereas D-Cy5 signal does not exhibit such correspondence. C) Cy5-D-DPA exhibits significantly greater colocalization coefficient with mitochondrial signal than D-Cy5. *** $p < 0.001$.

701x519mm (144 x 144 DPI)

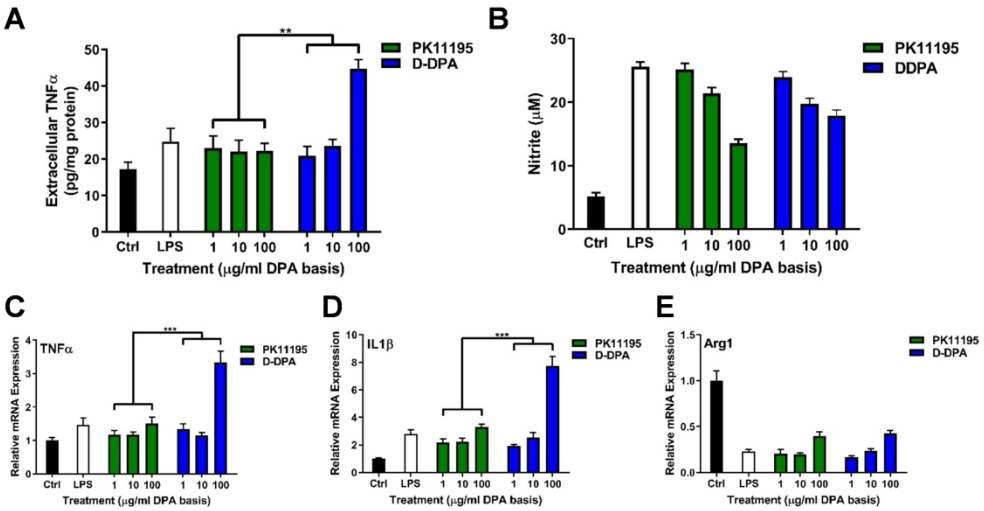

Figure 4. D-DPA treatment increases anti-tumor inflammatory signals. BV2 murine microglia were stimulated with LPS at 300 EU/mL for 3 hours, followed by cotreatment with PK11195 or DPA-conjugated dendrimer (D-DPA) for 24 hours. Then, cells were exposed to fresh media for 24 hours and collected for analyses of cellular and extracellular signals. A) Treatment with D-DPA significantly increases the secretion of TNFα, a tumor-killing signal, from stimulated BV2 microglia compared to PK11195 treatment. ** $p < 0.01$. B) Both treatments reduced secretion of nitrite, a reactive oxygen species indicative of oxidative stress. Analyses of mRNA expression via rt-qPCR demonstrates that D-DPA significantly increases expression of anti-tumor signals C) TNFα and D) IL1β while limiting expression of E) pro-tumor cytokine arginase-1 (Arg1). *** $p < 0.001$.

685x358mm (144 x 144 DPI)

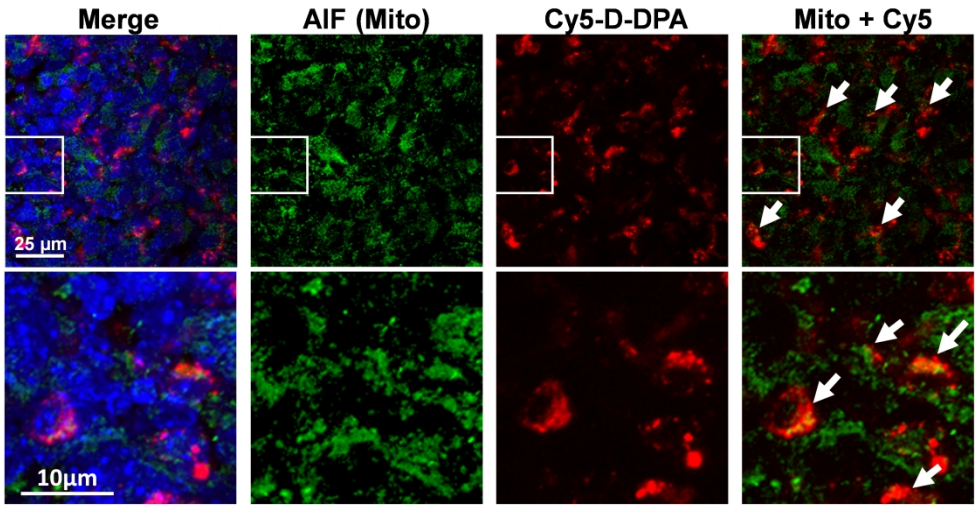

Figure 5. D-DPA targets mitochondria within the glioblastoma tumor. Glioblastoma brain tumor-bearing mice were injected intravenously with fluorescently labelled dendrimer-DPA conjugates (Cy5-D-DPA, red) 14 days after tumor inoculation. 24 hours after injection, brains were collected, fixed, and stained with DAPI to label cell nuclei (blue) and AIF to label mitochondria (Mito, green). Cy5-D-DPA targets mitochondria within the tumor (white arrows) in tumor-associated macrophages upon systemic administration. Localization with the nucleus as seen in the in vitro images was not observed in vivo.

638x340mm (144 x 144 DPI)

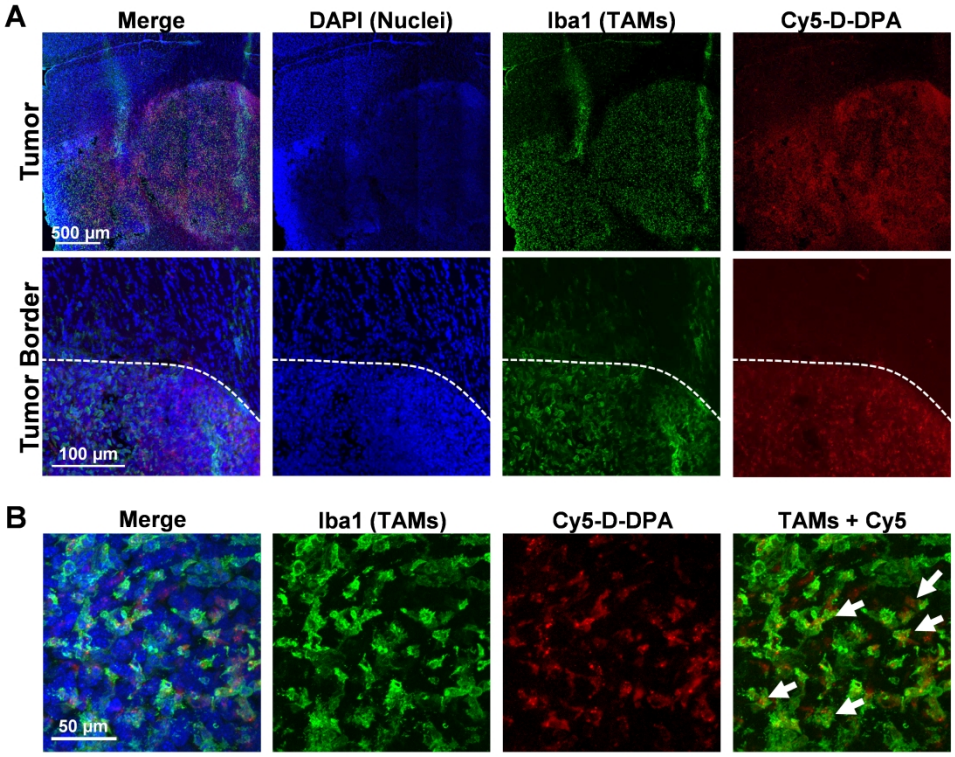

Figure 6. D-DPA specifically localizes to tumor-associated macrophages in the glioblastoma tumor upon systemic administration. Glioblastoma brain tumor-bearing mice were injected intravenously with fluorescently labelled dendrimer-DPA conjugates (Cy5-D-DPA, red) 14 days after tumor inoculation. 24 hours after injection, brains were collected, fixed, and stained with DAPI to label cell nuclei (blue) and Iba1 to label tumor-associated macrophages (TAMs, green) for confocal imaging. A) Whole tumor images (top panels) demonstrate that Cy5-D-DPA penetrates throughout the solid glioblastoma tumor after systemic administration. Imaging of the tumor border (bottom panels) demonstrate that Cy5-D-DPA localizes specifically within the tumor with high fidelity for the tumor border. B) Cy5-D-DPA signal colocalizes with Iba1 (white arrows), indicating specific targeting of TAMs within the glioblastoma tumor.

678x536mm (144 x 144 DPI)